



**HAL**  
open science

## Gibberellin and abscisic acid transporters facilitate endodermal suberin formation in Arabidopsis

Jenia Binenbaum, Nikolai Wulff, Lucie Camut, Kristian Kiradjiev, Moran Anfang, Iris Tal, Himabindu Vasuki, Yuqin Zhang, Lali Sakvarelidze-Achard, Jean-Michel Davière, et al.

► **To cite this version:**

Jenia Binenbaum, Nikolai Wulff, Lucie Camut, Kristian Kiradjiev, Moran Anfang, et al.. Gibberellin and abscisic acid transporters facilitate endodermal suberin formation in Arabidopsis. *Nature Plants*, 2023, 9 (5), pp.785-802. 10.1038/s41477-023-01391-3 . hal-04256214

**HAL Id: hal-04256214**

**<https://hal.science/hal-04256214v1>**

Submitted on 24 Oct 2023

**HAL** is a multi-disciplinary open access archive for the deposit and dissemination of scientific research documents, whether they are published or not. The documents may come from teaching and research institutions in France or abroad, or from public or private research centers.

L'archive ouverte pluridisciplinaire **HAL**, est destinée au dépôt et à la diffusion de documents scientifiques de niveau recherche, publiés ou non, émanant des établissements d'enseignement et de recherche français ou étrangers, des laboratoires publics ou privés.

1 **Gibberellin and abscisic acid transporters facilitate endodermal suberin formation in**  
2 ***Arabidopsis***

3 Jenia Binenbaum<sup>1</sup>, Nikolai Wulff<sup>2</sup>, Lucie Camut<sup>3</sup>, Kristian Kiradjiev<sup>4,5</sup>, Moran Anfang<sup>1</sup>, Iris Tal<sup>1</sup>, Himabindu  
4 Vasuki<sup>1,6</sup>, Yuqin Zhang<sup>1</sup>, Lali Sakvarelidze-Achard<sup>3</sup>, Jean-Michel Davière<sup>3</sup>, Dagmar Ripper<sup>7</sup>, Esther Carrera<sup>8</sup>,  
5 Ekaterina Manasherova<sup>9</sup>, Shir Ben Yaakov<sup>1</sup>, Shani Lazary<sup>1</sup>, Chengyao Hua<sup>2</sup>, Vlastimil Novak<sup>10</sup>, Christoph Crocoll<sup>2</sup>,  
6 Roy Weinstain<sup>1</sup>, Hagai Cohen<sup>9</sup>, Laura Ragni<sup>7</sup>, Asaph Aharoni<sup>6</sup>, Leah R Band<sup>4,5,✉</sup> Patrick Achard<sup>3,✉</sup> Hussam Hassan  
7 Nour-Eldin<sup>2,✉</sup> and Eilon Shani<sup>1,✉</sup>

8

9 <sup>1</sup> School of Plant Sciences and Food Security, Tel Aviv University, Tel Aviv, 69978, Israel.

10 <sup>2</sup> DynaMo Center of Excellence, Department of Plant and Environmental Sciences, University of Copenhagen,  
11 Frederiksberg, 1871, Denmark.

12 <sup>3</sup> Institut de Biologie Moléculaire des Plantes, CNRS, Université de Strasbourg, 67084, Strasbourg, France.

13 <sup>4</sup> Centre for Mathematical Medicine and Biology, School of Mathematical Sciences, University of Nottingham,  
14 Nottingham NG7 2RD, UK.

15 <sup>5</sup> Division of Plant and Crop Sciences, School of Biosciences, University of Nottingham, Sutton Bonington Campus,  
16 Loughborough LE12 5RD, UK.

17 <sup>6</sup> Department of Plant and Environmental Sciences, Weizmann Institute of Science, Rehovot 7610001, Israel.

18 <sup>7</sup> ZMBP-Center for Plant Molecular Biology, University of Tübingen, Tübingen, Germany.

19 <sup>8</sup> Instituto de Biología Molecular y Celular de Plantas, CSIC-UPV, Valencia, Spain.

20 <sup>9</sup> Department of Vegetable and Field Crops, Institute of Plant Sciences, Agricultural Research Organization (ARO),  
21 Volcani Center, Rishon Lezion 7505101, Israel.

22 <sup>10</sup> Plant Nutrients and Food Quality Research Group, Department of Plant and Environmental Sciences, University of  
23 Copenhagen, Frederiksberg, 1871, Denmark.

24 ✉ Corresponding author

25

26 **Abstract**

27 The plant hormone gibberellin (GA) regulates multiple developmental processes. It accumulates in the root  
28 elongating endodermis, but how it moves into this cell file and the significance of this accumulation are  
29 unclear. Here, we identified three NPF transporters required for GA and abscisic acid (ABA) translocation.  
30 We demonstrate that NPF2.14 is a subcellular GA/ABA transporter, the first to be identified in plants,  
31 facilitating GA and ABA accumulation in the root endodermis to regulate suberization. Further, NPF2.12  
32 and NPF2.13, closely related proteins, are plasma membrane-localized GA and ABA importers that  
33 facilitate shoot-to-root GA<sub>12</sub> translocation, regulating endodermal hormone accumulation. This work  
34 reveals that GA is required for root suberization and that GA and ABA can act non-antagonistically. We  
35 demonstrated how the clade of transporters mediates hormone flow with cell-file-specific vacuolar storage  
36 at the phloem unloading zone, and slow release of hormone to induce suberin formation in the maturation  
37 zone.

38

## 39 Introduction

40 The phytohormone gibberellin (GA) is essential for many developmental processes in plants. Among them  
41 are seed germination, organ elongation and expansion through cell growth and division, trichome  
42 development, the transition from vegetative to reproductive growth, and flower, seed, and fruit development  
43 <sup>1</sup>. GAs are produced mainly in the vasculature and move long distances in both acro- and basipetal directions  
44 <sup>2-5</sup>. The first reports of GA mobility through the phloem sap appeared over 50 years ago <sup>6-8</sup>. Grafting  
45 methods showed that biosynthesis of GA in the shoot can rescue GA biosynthesis mutations in the  
46 hypocotyl and root and *vice versa* <sup>6-8</sup>. In tobacco plants, defoliation results in an internode elongation,  
47 cambial activity, and fiber differentiation phenotypes that are similar to treatment with paclobutrazol, a GA  
48 biosynthesis inhibitor <sup>5</sup>. Another example of an organ dependent on an external source of GA are the petals,  
49 which require the anthers as their GA source <sup>9,10</sup>. The biosynthesis of active GA is a complex, multi-step  
50 process with diverse intermediates <sup>11</sup>. Regnault et al. conducted a series of grafting experiments using  
51 *Arabidopsis thaliana* mutant plants compromised at different stages of GA biosynthesis and identified GA<sub>12</sub>  
52 as the major GA form transported over a long distance through the vasculature <sup>12</sup>. GA<sub>12</sub> moves through the  
53 xylem in a root-to-shoot manner and in the phloem in a shoot-to-root direction to regulate plant growth <sup>12</sup>.  
54 The translocation of GA<sub>12</sub> from the root to the shoot is enhanced under ambient temperatures to induce  
55 shoot growth <sup>13</sup>. The transporters that regulate GA long-distance transport in the plant remain unknown.

56 In recent years, a number of *Arabidopsis* GA plasma membrane importers have been identified, two from  
57 the SWEET family and several others from the NITRATE TRANSPORTER1/PEPTIDE TRANSPORTER  
58 (NPF) family <sup>14-17</sup>. There are 53 NPFs in *Arabidopsis*, divided into eight subfamilies. These proteins are  
59 capable of transporting a large variety of substrates such as nitrate, glucosinolates, abscisic acid (ABA),  
60 auxin, and GAs <sup>14,18,19</sup>. Like auxin, GA is subjected to the ion-trap mechanism, limiting its ability to move  
61 out of cells. The existence of GA efflux transporters is therefore predicted to allow GA cell-to-cell  
62 movement <sup>20</sup>; however, no GA efflux transporters have been discovered <sup>21</sup>.

63 ABA, which regulates growth and stress responses, has been long thought to act antagonistically to GA in  
64 processes such as seed germination, seed maturation, and dormancy and in responses to external cues <sup>22-24</sup>.  
65 Both GA and ABA induce developmental responses specifically from the endodermis <sup>25-27</sup>. GA accumulates  
66 at high levels in the endodermal cells of the root elongation zone <sup>28</sup>. The process is dependent on the activity  
67 of NPF3.1 (NPF3), a member of the NPF family, which has been shown to act as a dual-specificity GA and  
68 ABA importer <sup>16,29</sup>. The endodermis, the innermost cortical layer that surrounds the central vasculature,  
69 goes through two phases of differentiation: The first step involves polar localized lignin deposition, which  
70 results in the formation of the casparian strips, and the second is the deposition of suberin as a lamella

71 below the primary cell wall<sup>30</sup>. The casparian strips restrict apoplastic diffusion of water and nutrients into  
72 the vascular tissues, whereas suberin limits backflow of nutrients from the stele<sup>31,32</sup>. The physiological  
73 relevance of GA accumulation in the endodermis remains unknown.

74 With this study, we identified a sub-clade of NPF transporters that orchestrate GA<sub>12</sub> long-distance shoot-  
75 to-root translocation and promote bioactive ABA and GA movement from the vasculature to the  
76 endodermis, which is required for endodermal suberization, a phenotype rescued by applying either ABA  
77 or GA. The importance of transporter distributions was evaluated via a multicellular mathematical model  
78 that suggest an intriguing slow-release mechanism whereby GA and ABA delivered to the root in the  
79 phloem unloading zone are loaded into pericycle vacuoles and then slowly released to induce suberin  
80 formation in the maturation zone. Together, our findings reveal the mechanism that facilitates long-distance  
81 shoot-to-root movement of GA<sub>12</sub> and explain how bioactive GA<sub>4</sub> and ABA are transported from the  
82 vasculature to the endodermis to mediate endodermal suberization.

83

## 84 **Results**

### 85 **NPF2.14 is a tonoplast-localized GA and ABA transporter**

86 To identify the missing GA exporters in plants, we tested whether NPF proteins were capable of GA<sub>4</sub> export  
87 in *Xenopus laevis* oocyte-based transport assays. All other GA transporters identified to date import GA  
88<sup>14,33</sup>. The transport assays investigate whether NPFs lead to efflux of GA that is loaded into oocytes by three  
89 different approaches, namely diffusion, injection and import by a GA importer. Oocytes expressing various  
90 *NPFs* or control oocytes injected with water were exposed to an array of membrane-permeable GAs (GA<sub>4</sub>,  
91 GA<sub>7</sub>, GA<sub>9</sub> and GA<sub>12</sub>)<sup>34</sup>. The screen has identified NPF2.14 as a potential GA exporter. At the end of assay,  
92 NPF2.14-expressing oocytes contained significantly reduced GA levels compared to control oocytes (**Fig.**  
93 **1a**). This suggests that NPF2.14 facilitates the export activity of GAs out of oocytes. This was confirmed  
94 in an injection-based assay in which GA<sub>3</sub>, a non-membrane-permeable form of GA, was injected directly  
95 into the oocyte. At the end of the assay, there was a lower GA<sub>3</sub> content in NPF2.14-expressing oocytes  
96 compared to control oocytes (**Fig. 1b**). Co-expression of both *NPF2.14* RNA and *NPF4.1*, which encodes  
97 a known GA importer, led to a reduced accumulation of non-membrane permeable GA<sub>3</sub> compared to  
98 oocytes expressing only *NPF4.1* (**Fig. 1c**), further supporting that NPF2.14 exports GA out of *Xenopus*  
99 *laevis* oocytes.

100 It was previously shown that NPF3.1 transports both GA and ABA in *Xenopus laevis* oocytes<sup>16</sup>. To test  
101 whether NPF2.14 also has dual-substrate specificity, control and NPF2.14-expressing oocytes were

102 exposed to ABA. NPF2.14-expressing oocytes accumulated less ABA than did control oocytes (**Fig. 1d**),  
103 indicating that NPF2.14 has dual-substrate transport activity. Several NPF transporters, including NPF6.3,  
104 also transport nitrate<sup>18</sup>, but NPF2.14 displayed no nitrate transport activity in oocyte assays (**Fig. 1e**).

105 Wulff et al. recently showed that NPF7.3 lowers the cytoplasmic pH in *Xenopus laevis* oocytes, which can  
106 indirectly influence the accumulation equilibrium of weak acids such as GA and ABA<sup>34</sup>. In order to assess  
107 whether NPF2.14 has a similar activity, we measured the intracellular oocyte pH using a proton-selective  
108 three-electrode voltage clamp setup. We showed that, unlike NPF7.3, NPF2.14 expression in the oocyte  
109 does not alter the internal oocyte pH (**Fig. 1f**). Another factor that theoretically can lead to a false-positive  
110 GA export result is alteration of membrane potential. Therefore, we measured the membrane potential of  
111 control and NPF2.14-expressing oocytes using a two-electrode voltage clamp setup. The membrane  
112 potential of control and NPF2.14-expressing oocytes were both approximately -15 mV (**Fig. 1g**). When  
113 oocytes were subjected to GA<sub>4</sub> for 60 min prior to membrane potential measurement, less GA was observed  
114 in NPF2.14-expressing oocytes than control oocytes (**Fig. 1g**). Thus, NPF2.14 does not shift oocyte  
115 membrane potential.

116 Many NPF proteins, including NPF2.14, contain the ExxE[K/R] motif<sup>35</sup>, which is involved in coupling  
117 substrate transport to the proton gradient across membranes<sup>36</sup>. Involvement of the ExxE[K/R] motif in  
118 NPF2.14-mediated effluxes would suggest antiporter function. To assess the involvement of the ExxE[K/R]  
119 motif, we generated C-terminal YFP-tagged NPF2.14 mutants substituted at each of the three charged  
120 residues with a polar but uncharged residue. The YFP-tag alone did not influence the apparent GA<sub>4</sub> transport  
121 by the wild-type NPF2.14 (**Fig. 1h**). When any of the charged residues of the ExxE[K/R] motif was replaced  
122 with the polar uncharged Gln residue, no significant difference in GA<sub>4</sub> transport was observed compared to  
123 wild-type NPF2.14 (**Fig. 1h**). Thus, the GA<sub>4</sub> transport mediated by NPF2.14 seems to be ExxE[K/R] motif  
124 independent.

125 In order to test whether the *Xenopus laevis* oocyte GA transport data is physiologically relevant *in planta*,  
126 we isolated a homozygous T-DNA knockout line for *NPF2.14*. The single *npf2.14* mutant did not show  
127 significant shoot or root growth phenotypes (**Sup. Fig. 1a-b**). Several NPF family members transport  
128 nitrate, including NPF6.3<sup>37</sup>. Thus, despite having shown that NPF2.14 does not transport nitrate in oocytes  
129 (**Fig. 1d**), we checked whether *npf2.14* mutants display an impaired growth on low nitrate media. *npf2.14*  
130 T-DNA insertion mutants did not have a visible growth phenotype and did not differ from Col-0 plants  
131 under low nitrate conditions (**Sup. Fig. 1c**). To determine whether NPF2.14 is involved in GA distribution  
132 and accumulation in the root, we tested whether the distribution of a fluorescently tagged GA<sub>3</sub> compound  
133 (GA<sub>3</sub>-Fl) was affected in the loss-of-function line. GA<sub>3</sub>-Fl has been developed in our lab to serve as a stable,

134 bioactive reporter to study GA movement/accumulation *in planta*<sup>28</sup>. Accumulation of GA<sub>3</sub>-Fl in the  
135 endodermis was visible in the Col-0 plants, as previously shown<sup>28</sup>. The *npf2.14* mutants displayed a  
136 significantly stronger signal compared to the Col-0 control (**Fig. 1i**). This enhanced accumulation was  
137 restored to normal levels when expressing *NPF2.14* driven by its native promoter (*pNPF2.14:NPF2.14-*  
138 *GFP*) on the background of the *npf2.14* T-DNA line (**Fig. 1i**), indicating that loss of NPF2.14 affects GA<sub>3</sub>-  
139 Fl distribution in the plant. In agreement with this result, *npf2.14* mutants accumulated significantly higher  
140 levels of GA<sub>4</sub> in their roots (**Fig. 1j**).

141 To test whether NPF2.14 has a dual specificity function and can also import ABA, we tested the distribution  
142 of the fluorescently tagged ABA (ABA-Fl) in the roots. ABA-Fl is non-bioactive but can be utilized to  
143 estimate ABA movement in the plant<sup>33</sup>. In addition, we quantified endogenous levels of ABA in the roots.  
144 We found that similarly to GA-Fl, *npf2.14* mutants accumulated significantly high levels of ABA-Fl in their  
145 root endodermis cells (**Sup. Fig. 2**), but showed low levels of native ABA (extracted from the entire root)  
146 (**Fig. 1j**).

147 In order to study the subcellular localization of NPF2.14, we generated and imaged *35S:NPF2.14-YFP*  
148 lines. Interestingly, NPF2.14 localized to the tonoplast vacuole membrane (**Fig. 1k**). Therefore, although  
149 we had hypothesized that NPF2.14 was a GA exporter that transported GA from inside the cytosol to the  
150 apoplast, the protein is instead a tonoplast-localized transporter. To the best of our knowledge, this is the  
151 first report of a sub-cellular GA/ABA transporter.

152

### 153 **NPF2.14 regulates suberin formation in the root endodermis**

154 To characterize NPF2.14 expression patterns in the plant, we generated NLS-YFP and GUS reporter lines  
155 driven by the *NPF2.14* promoter. Confocal imaging of the NLS-YFP lines indicated that NPF2.14 is  
156 expressed only in the pericycle of the root mature zone, mainly at the phloem poles, and not in the  
157 meristematic zone (**Fig. 2a, Sup. Fig. 3a**). In addition, GUS staining showed expression in the shoot  
158 vasculature in seedlings (**Sup. Fig. 3b**). To test if GA or ABA affects NPF2.14 expression patterns, we  
159 examined *pNPF2.14:GUS* lines after an exogenous treatment of GA<sub>3</sub> (5 μM) or ABA (1 μM). While GA  
160 did not affect *pNPF2.14:GUS* staining, we observed a stronger staining in the ABA treatment, yet  
161 expression remained in the vasculature (**Sup. Fig. 4**). In the mature stages, the *NPF2.14*-driven reporter  
162 was expressed in the periderm (**Sup. Fig. 3c**). The pericycle is a deep layer of post-embryonic meristematic  
163 cells encircling the vascular tissue<sup>38</sup>. In the root, it is required for lateral root emergence<sup>39</sup>, xylem loading  
164<sup>40</sup> and phloem unloading<sup>41</sup>. At later stages it gives rise to the periderm, which serves as the outer protective

165 layer when the surrounding tissue is sloughed off <sup>38</sup>. Both the endodermis and the cork, which is the  
166 outermost cell layer of the periderm are suberized tissues <sup>42</sup>.

167 The expression of the reporter driven by the *NPF2.14* promoter in a tissue that undergo suberization, taken  
168 together with the ability of NPF2.14 to transport ABA, which has been previously shown to regulate suberin  
169 deposition <sup>43</sup>, led us to hypothesize that this transporter might facilitate root suberization.

170 To test this, we analyzed suberization in *npf2.14* T-DNA mutants using Nile red and Fluorol yellow, which  
171 are suberin dyes <sup>44,45</sup>. Suberization commences in the endodermis of the upper part of the maturation zone  
172 of the root, and, as the plant matures more cells undergo suberization <sup>46</sup>. Quantification of Nile red and  
173 Fluorol yellow fluorescence intensity in the uppermost part of 5-day-old roots revealed that the mutant  
174 *npf2.14* plants had significantly lower levels of endodermal suberin than Col-0 plants (**Fig. 2b, Sup. Fig.**  
175 **5**). In addition, Col-0 plants roots showed a typical pattern of suberin formation with a non-suberized zone,  
176 followed by a suberizing zone where only patches of endodermal cells are suberized (patchy suberization)  
177 and a continuous suberized zone. We found significant reduction in the continuously suberized zone for  
178 *npf2.14* T-DNA, and an additional CRISPR *npf2.14* allele we generated (**Fig. 2c**). Suberin levels remained  
179 lower compared to Col-0 at later stages of development, including 10-day-old roots and 3-week-old  
180 hypocotyls (**Sup. Fig. 6**), showing that the reduction of suberin deposition in the endodermis is stable over  
181 time and that also cork suberin is affected.

182 Suberin is a complex polyester based on glycerol and long-chain  $\alpha,\omega$ -diacids and  $\omega$ -hydroxyacids <sup>47</sup>, which  
183 is primarily found in structures such as the periderm, endodermis, and seed coat <sup>30</sup>. To examine changes in  
184 root suberin composition between *npf2.14* and Col-0, we analyzed their suberin monomer profiles via gas  
185 chromatography-mass spectrometry (GC-MS). We found significant reductions in ferulic acid, the  
186 predominant aromatic component of suberin, as well as in C22 fatty acid and C18:1(9)  $\omega$ -hydroxyacid, two  
187 of the most abundant suberin building blocks in the Arabidopsis root endodermis (**Fig. 2d**). In addition,  
188 C18 ester was lower in *npf2.14* roots. These reductions accompanied by lower levels of other monomers  
189 resulted in 35% less total suberin contents in the mutant roots (**Fig. 2d**). Overall, the findings provide several  
190 lines of evidence that alteration of NPF2.14 has a substantial effect on suberin deposition in the root  
191 endodermis.

192 Similar to the *npf2.14* mutant, *npf3.1* mutant plants, which have been shown to have impaired GA and ABA  
193 delivery to the endodermis <sup>16</sup>, displayed reduced suberization levels compared to Col-0 plants (**Sup. Fig.**  
194 **7**). GA and ABA treatments completely rescued the *npf2.14* mutant suberization levels (**Fig. 2b**).



195 Endodermal suberization is regulated by ABA perception, both under normal and stress conditions <sup>48,49</sup>.  
196 ABA treatment was previously reported to induce endodermal suberization <sup>50</sup>. In agreement with this report,  
197 ABA significantly upregulated the Nile red fluorescence intensity in the root endodermis and rescued the  
198 reduced suberization observed in the *aba2-1* mutant, which is deficient in ABA biosynthesis <sup>50</sup> (**Fig. 2e**).  
199 To the best of our knowledge, GA has not been previously associated with endodermal suberization. To  
200 establish whether or not GA regulates root suberization in *Arabidopsis* seedlings, we quantified suberization  
201 levels in GA-treated wild-type and *gal-13* mutant plants using the Nile red dye. GA1 catalyzes the first  
202 committed step in the GA biosynthetic pathway <sup>51</sup>. The GA biosynthesis mutant *gal-13* displayed a  
203 significant reduction in suberization levels, which was restored by the exogenous application of GA<sub>3</sub> (**Fig.**  
204 **2f**). Furthermore, while ABA treatment, but not GA treatment, can rescue and induce the reduced suberin  
205 levels of *aba2-1*, both ABA and GA can rescue the reduced suberin levels of *gal-13* (**Fig. 2e-f**). Notably,  
206 GA treatment could only rescue the suberin back to WT levels, and did not induce it to a higher level as  
207 ABA treatment did. GA and ABA have long been thought to have completely antagonistic functions <sup>52</sup>. Our  
208 results indicate that this antagonistic activity is more complex and that GA and ABA induce root  
209 suberization. Taken together, our data suggest that NPF2.14 is a pericycle-specific GA and ABA  
210 transporter, localized to the tonoplast, and involved in regulating GA and ABA accumulation in the  
211 endodermis to promote suberization.

212

### 213 **NPF2.12 and NPF2.13 are plasma membrane-localized GA and ABA importers**

214 *NPF2.12* and its close paralog *NPF2.13* form a phylogenetic sub-clade with *NPF2.14* (**Fig. 3a, Sup. Fig.**  
215 **8**). We hypothesized that due to this proximity on the phylogenetic tree, NPF2.12 and NPF2.13 might also  
216 contribute to GA and ABA accumulation in the endodermis. Both transporters were previously  
217 characterized as low-affinity nitrate transporters <sup>53,54</sup> and more recently, were shown to promote GA import  
218 activity in heterologous systems <sup>14,34</sup>. Neither have been characterized in plants as GA or ABA transporters.  
219 To test for direct GA transport activity of NPF2.12 and NPF2.13, we performed *Xenopus laevis* oocyte-  
220 based transport assays. Oocytes expressing NPF2.12 or NPF2.13 accumulated significantly higher levels  
221 of GA<sub>1</sub>, GA<sub>3</sub>, GA<sub>4</sub>, GA<sub>7</sub>, GA<sub>9</sub>, GA<sub>12</sub>, GA<sub>19</sub>, and GA<sub>24</sub> compared to control oocytes over the course of 60  
222 min (**Fig. 3b, Sup. Fig. 9a**). This suggests that NPF2.12 and NPF2.13 are promiscuous GA importers. Both  
223 NPF2.12- and NPF2.13-expressing oocytes also had higher levels of ABA accumulation than controls (**Fig.**  
224 **3c**).

225 NPF2.12 and NPF2.13 both contain an ExxE[K/R] motif, which couples the substrate transport to the proton  
226 gradient <sup>36</sup>. To test whether NPF2.12 and NPF2.13 substrate transport activity is coupled with external

227 proton concentration, NPF2.12- and NPF2.13-expressing oocytes were exposed to membrane-impermeable  
228 GA<sub>1</sub> in solutions ranging from pH 5 to 7 in 0.5 pH unit increments. In both NPF2.12- and NPF2.13-  
229 expressing oocytes, GA<sub>1</sub> accumulation increased as pH was lowered. (**Fig. 3d**). These data indicate that GA  
230 transport by NPF2.12 and NPF2.13 is likely proton-coupled.

231 To investigate whether the transport of GA by NPF2.12 and NPF2.13 is electrogenic, we used two-electrode  
232 voltage clamp electrophysiology (TEVC) to evaluate oocytes that express the transporters. Subtracting the  
233 currents elicited by oocytes at different membrane potentials in the absence of GAs from the currents  
234 elicited by oocytes in the presence of 500 μM GA<sub>3</sub> revealed that GA<sub>3</sub> transport by both NPF2.12 and  
235 NPF2.13 is associated with negative currents relative to control oocytes (**Fig. 3e**). As the negative currents  
236 reflect a net positive influx of charges, this indicates at least a 2:1 proton:GA<sub>3</sub> stoichiometry if GA<sub>3</sub> is  
237 transported in its anionic form. However, it cannot be excluded that GA<sub>3</sub> may be transported in its neutral  
238 form. In non-clamped conditions, NPF2.13 displayed significantly higher uptake levels of GA<sub>1</sub> and GA<sub>4</sub>  
239 compared to NPF2.12. Similarly, currents elicited by NPF2.13-expressing oocytes were significantly higher  
240 compared to NPF2.12-expressing oocytes when oocytes were clamped at membrane potentials that mimic  
241 the membrane potential in the non-clamped uptake assays (Fig 3e, f). However, at high negative membrane  
242 potential (-120 mV), GA<sub>3</sub>, induced-currents in NPF2.12-expressing oocytes were of the same magnitude as  
243 those of NPF2.13-expressing oocytes (**Fig. 3e, f**). This suggests that the transport activity of NPF2.12 is  
244 sensitive to alternations in the membrane potential (**Fig. 2b**). In agreement with previous publications<sup>53,54</sup>,  
245 we detected nitrate import into oocytes that expressed NPF2.12 or NPF2.13, but this transport did not  
246 interfere with the GA transport capabilities as GA accumulation was not affected in GA/nitrate competition  
247 assays (**Sup. Fig. 9b**). In continuation, we performed equimolar GA/ABA competition transport assays,  
248 which showed ABA does not affect GA transport, whereas a slight but significant enhancement in ABA  
249 uptake was seen in NPF2.13-expressing oocytes when exposed simultaneously to GA<sub>3</sub>. The data shows that  
250 NPF2.12 and NPF2.13 are multi-specific towards nitrate, ABA and GA and suggests that GA might  
251 enhance NPF2.13 ABA transport activity (**Sup. Fig. 10**). Multi-specificity has emerged as an inherent  
252 property of the NPF family that is suggested to enable the tantalizing integration of environmental  
253 information to the availability of the different nutrients<sup>18</sup>. Exhaustive structure–function studies are needed  
254 to decipher the molecular basis of the selectivity of these transporters.

255 To elucidate whether these transporters are part of the GA transport mechanisms in the plant, we treated T-  
256 DNA knockout lines, which did not display any visible phenotypes (**Sup. Fig. 11**), with GA<sub>4</sub>-Fl. *npf2.12*  
257 and *npf2.13* single mutant plants treated with GA<sub>4</sub>-Fl displayed a significant reduction in accumulation in  
258 the endodermis compared to Col-0 plants (**Fig. 3g**), similar to reduced levels detected in *npf3.1* mutants.  
259 To verify that the reduction in GA-Fl accumulation was not due to an off-target mutation, we repeated the

260 test with an additional *npf2.12* T-DNA insertion line (*npf2.12-2*) and obtained similar results (**Sup. Fig.**  
261 **12a**). In addition, homozygous *pNPF2.13:NPF2.13-YFP* plants completely rescued the root GA<sub>3</sub>-Fl  
262 phenotype (**Sup. Fig. 12b**).

263 We next generated plants ectopically expressing *NPF2.12* and *NPF2.13* fused to YFP (*p35S:NPF2.12-YFP*  
264 and *p35S:NPF2.13-YFP*, respectively) and treated them with GA<sub>3</sub>-Fl. These lines showed a remarkably  
265 strong accumulation of GA<sub>3</sub>-Fl in all root cells (**Fig. 3h**), supporting the hypothesis that NPF2.12 and  
266 NPF2.13 are GA transporters *in planta*. In order to test whether NPF2.12 and NPF2.13 have a dual  
267 specificity function and can also import ABA (such as NPF2.14), we treated plants with fluorescently  
268 tagged ABA (ABA-Fl) <sup>33</sup>. Overexpression of NPF2.12 or of NPF2.13 resulted in extreme ABA-Fl  
269 accumulation compared to Col-0 plants (**Fig. 3h**), implying that both transporters import GA and ABA *in*  
270 *planta*.

271 Finally, in order to address the subcellular localization of NPF2.12 and NPF2.13, we imaged the root  
272 epidermis cells of *p35S:NPF2.12-YFP* and *p35S:NPF2.13-YFP* lines. Both NPF2.12 and NPF2.13 are  
273 localized to the plasma membrane (**Fig. 3i**). Together, the *in planta* and oocyte results indicate that NPF2.12  
274 and NPF2.13 are dual-substrate, plasma membrane-localized GA and ABA importers.

275

## 276 **NPF2.12 and NPF2.13 regulate root suberization**

277 To further elucidate the biological function of NPF2.12 and NPF2.13, we generated NLS-YFP and GUS  
278 reporter lines to map NPF2.12 and NPF2.13 expression patterns. Confocal microscopy of plants expressing  
279 *NLS-YFP* driven by *NPF2.12* and *NPF2.13* native promoters revealed that in the root, NPF2.12 was  
280 expressed in the pericycle of the whole root and subsequently in the periderm of mature plants; NPF2.13,  
281 on the other hand, was expressed only in the shoot (**Fig. 4a, Sup. Fig. 13**). Analysis of *pNPF2.12:GUS* and  
282 *pNPF2.13:GUS* lines showed that the two transporters are expressed in the shoot vasculature (**Fig. 4b**). GA  
283 or ABA treatment did not have a major effect on *NPF2.12* and *NPF2.13* expression level, detected by qPCR  
284 and GUS reporter lines (**Sup. Fig. 14**). The fact that the *NPF2.13* translational fusion construct  
285 (*pNPF2.13:NPF2.13-Venus*) introduced into the *npf2.13* mutant background rescued the root GA<sub>3</sub>-Fl  
286 accumulation phenotype indicated that the promoter region we cloned is sufficient and that NPF2.13  
287 expression is restricted to the shoot (**Sup. Fig. 12b**). Similar to *npf2.14* mutants, *npf2.12* and *npf2.13* mutant  
288 plants displayed a reduction in suberization. Mutant roots stained with Nile red or Fluorol yellow showed  
289 a weaker fluorescence intensity than detected in Col-0 plants (**Fig. 4c, Sup. Fig. 15**). In agreement,  
290 additional mutant alleles for *npf2.12* and *npf2.13* showed reduction in suberin level and patterning (**Sup.**  
291 **Fig. 16**). Similar to *npf2.14* mutants, we detected a reduction in endodermal suberin levels of *npf2.12* and

292 *npf2.13* 10-day-old roots and a lower levels of cork suberin in 3-week-old *npf2.12 npf2.13* double mutant  
293 hypocotyls stained with Fluorol yellow (**Sup. Fig. 17**).

294 In order to test if *NPF2.12* and *NPF.13* have partially redundant activities, we generated the *npf2.12 npf2.13*  
295 double mutant. The phenotype of the *npf2.12 npf2.13* double mutant line was not enhanced compared to  
296 the single *npf2.12* and *npf2.13* mutants (**Fig. 4c-d**). We further generated additional double and triple mutant  
297 combinations with the *npf2.14* mutant via CRISPR genome editing (as *NPF2.14* is genetically linked to  
298 *NPF2.13*), and tested their activity. We analyzed suberin patterning for all genotypes and found that the  
299 phenotypes of the higher order mutant knockouts were not enhanced compared to the single mutants (**Sup.**  
300 **Fig. 18**). This result is in line with the fact that there is limited overlap between the three genes in terms of  
301 expression pattern or protein localization. Notably, GA<sub>3</sub> or ABA treatment completely rescued *npf2.12* low-  
302 suberin phenotype. The phenotypes of *npf2.13* and of the *npf2.12 npf2.13* double mutant were completely  
303 rescued by ABA and largely rescued by GA<sub>3</sub> (**Fig. 4c**). Quantification of suberin monomer content revealed  
304 that both *npf2.12* and *npf2.13* mutant roots accumulated ~40% less total suberin contents compared to the  
305 Col-0 attributed to lower levels of vanillic and ferulic acids, C22 fatty acid, C20 fatty alcohol, and C18:1(9),  
306 C22 and C26  $\alpha$ -hydroxyacids (**Fig. 4e**).

307

### 308 **NPF2.12 and NPF2.13 regulate shoot-to-root GA translocation**

309 Our previous work showed that GA<sub>12</sub>, though not bioactive, is the primary GA form transported over long  
310 distances through the vasculature in *Arabidopsis thaliana*<sup>55</sup>. GA<sub>12</sub> can move through the xylem in a root-  
311 to-shoot manner and in the phloem in a shoot-to-root direction to regulate adaptive plant growth<sup>12,13</sup>.  
312 However, the mechanism regulating this process remains unknown<sup>21</sup>. *NPF2.13* was expressed strictly in  
313 the shoot (**Fig. 4a, b**), yet the knockout led to a phenotype in the root endodermis (**Fig. 4c**). This led us to  
314 hypothesize that the transporters are involved in the long-distance shoot-to-root translocation of GA. To  
315 test whether *NPF2.12* and *NPF2.13* facilitate shoot-born GA loading into the phloem, we quantified GA  
316 content in phloem exudates collected from leaf petioles. The double *npf2.12 npf2.13* loss-of-function  
317 mutant showed a striking reduction in GA<sub>12</sub> content in the collected phloem exudates (**Fig. 5a**). Other GA  
318 metabolites (GA<sub>15</sub>, GA<sub>24</sub>, GA<sub>9</sub>, GA<sub>4</sub>, GA<sub>34</sub>, and GA<sub>51</sub>) were not significantly reduced (**Fig. 5a**). ABA levels  
319 showed a mild decrease, significant when compared to Col-0 using two-tailed t-tests but not significant  
320 when using Dunnett's multiple comparisons test ( $p \leq 0.05$ ). The results imply that *NPF2.12* and *NPF2.13*  
321 regulate GA, and possibly ABA, loading into the shoot phloem. In agreement, quantification of active GA<sub>4</sub>  
322 content in the root, which is downstream to GA<sub>12</sub> in the biosynthesis pathway, showed a significant

323 reduction in the *npf2.12* and *npf2.13* single and double mutant lines (**Fig. 5b**). ABA content was also  
324 significantly lower in mutant roots compared to Col-0 (**Fig. 5b**).

325 To further test this hypothesis, we examined the expression pattern of the two transporters using reporter  
326 lines. In mature rosette, *NPF2.12* and *NPF2.13* were expressed in the shoot apex and the main vascular  
327 vein (**Fig. 5c**). Cross-sections of *pNPF2.12:GUS* and *pNPF2.13:GUS* leaf petioles showed that both genes  
328 were expressed in the phloem companion cells (**Fig. 5c**). Next, we investigated whether these transporters  
329 are involved in long-distance GA movement from the shoot to the root. For this purpose, 16-day-old plants  
330 were grown on paclobutrazol, a GA biosynthesis inhibitor, for 4 days to deplete the plants of native GA,  
331 and GA<sub>12</sub> was applied to a single leaf. We then quantified the abundance of the DELLA growth repressing  
332 protein REPRESSOR OF GA1-3 (RGA) in the root. DELLA proteins are central inhibitors of GA-regulated  
333 processes and GA relieves their inhibiting activity by activating their degradation<sup>56</sup>. Time-course  
334 experiments in Col-0 plants showed a significant reduction in RGA accumulation in the root after GA<sub>12</sub>  
335 treatment, indicating GA<sub>12</sub> movement from the shoot to the root (**Fig. d**). On the other hand, in the *npf2.12*  
336 *npf2.13* double mutant, RGA abundance remained stable (**Fig. 5d**), signifying a reduced GA accumulation  
337 in the root.

338 To understand how the NPF2.12/2.13/2.14-mediated long-distance GA transport influences root growth  
339 and suberin formation, we performed a series of micrograftings between Col-0, different combinations of  
340 *npf* double mutants and GA-deficient *gal-3* mutants and quantified both root elongation rate and Nile red  
341 fluorescence intensity. As expected, *gal-3* self-grafts had shorter roots and displayed a significantly lower  
342 Nile red fluorescence intensity than the Col-0 self-grafts (**Fig. 5e, Sup. Fig. 19**). Remarkably, *gal-3* roots  
343 grafted to Col-0 shoots were indistinguishable from that of Col-0 self-grafts (**Fig. 5e**), supporting our  
344 hypothesis that GA can be transported from the shoot to the root to induce suberin formation. In comparison,  
345 *gal-3* roots grafted to *npf2.12 npf2.13* shoots (*gal-3/npf2.12 npf2.13*) were smaller and showed a reduction  
346 in suberization levels compared to *gal-3/Col-0*, indicating a partial requirement of NPF2.12 and NPF2.13  
347 in long-distance GA transport (**Fig. 5e, Sup. Fig. 19**). Similarly, *npf2.12 npf2.14* and *npf2.13 npf2.14* double  
348 mutant's shoots grafted to *gal-3* roots, showed reduced suberin levels compared to *gal-3/Col-0*. In  
349 addition, we found that GA<sub>3</sub>-Fl application, specifically to the shoots of *npf2.12 npf2.14* double mutant or  
350 *npf2.14*, resulted in lower levels of GA<sub>3</sub>-Fl in the roots of seedlings growing on paclobutrazol (**Sup. Fig.**  
351 **20**). The results further suggest that NPF2.12/13/14 contribute to long-distance, shoot-to-root, GA  
352 translocation.

353 We hypothesize that once GA<sub>12</sub> is translocated to the roots, it can be converted to the bioactive GA<sub>4</sub> by the  
354 GA20ox and GA3ox enzymes, which are expressed in the root<sup>57</sup>. Profiling the expression pattern of the  
355 *GA3ox* promoters, catalyzing the last step in bioactive GA<sub>4</sub> hormone synthesis, showed that expression of

356 these enzymes is restricted to the stele as previously reported<sup>57</sup> (**Fig. 5f**). Together, these results imply that  
357 NPF2.12 and NPF2.13 function in GA<sub>12</sub> loading into the phloem for long-distance transport from the shoot  
358 to the root, with conversion to GA<sub>4</sub> taking place in the root stele.

359

360 **Pericycle-specific vacuolar storage of GA and ABA at the phloem unloading zone facilitates**  
361 **endodermal suberin induction in the maturation zone.**

362 To broaden our knowledge of GA and ABA distribution in the root and how it affects suberization, we  
363 created a mathematical model to simulate hormone distributions within the root cross-section, extending a  
364 modeling framework previously developed to study auxin transport<sup>58</sup>. Using a multicellular template  
365 segmented from a root-cross-sectional image (**Sup. Fig. 20**), we incorporated into the model experimentally  
366 observed transporter distributions: NPF3.1 on endodermal cell membranes<sup>16,29</sup>, NPF2.12 on pericycle cell  
367 membranes (**Fig. 3i, 4a**), and NPF2.14 on the pericycle tonoplasts (**Fig. 1k, 2a**). The model simulated active  
368 hormone transport via NPF3.1, NPF2.12, and NPF2.14, passive hormone transport across both plasma  
369 membrane and tonoplast, hormone synthesis and degradation, and hormone diffusion within the apoplast  
370 with significantly reduced diffusion in the endodermal apoplast due to the presence of the Casparian strip.  
371 To parameterize the model, permeabilities associated with each passive and active transport component  
372 were estimated using the oocyte data, and transport rates were then specified based on established pH and  
373 membrane potential values for plant cells<sup>58-60</sup> (**Sup. Table 5**). An important factor is the source of the  
374 hormone. *ABA2* and *AAO3*, which encode enzymes necessary for ABA biosynthesis, were previously  
375 shown to be expressed in the vasculature<sup>61</sup>. Bioactive GA<sub>4</sub> is also synthesized at high levels in the  
376 *Arabidopsis* stele<sup>57</sup> (**Fig. 5f**). Considering these data, together with the phloem unloading zone<sup>41</sup>, the  
377 docking belt for the long-distance shoot-to-root transported hormones, led us to specify the stele as the  
378 source of active GA and ABA in the model.

379 We first used the model to test the hypothesis that the discovered clade of transporters is necessary and  
380 sufficient to explain the observed endodermal hormone accumulation. With all transporters present, the  
381 model predicts high levels of both cytoplasmic and vacuolar hormone in the endodermis (**Fig. 6a for GA**  
382 **and Sup. Fig. 21**), consistent with the wildtype GA-FI and ABA-FI observations (**Fig. 1i, Sup. Fig. 2**)<sup>16</sup>  
383 and where suberization later occurs. Mutations in *npf3.1* and *npf2.12* were predicted to have reduced  
384 endodermal hormone cytoplasmic concentrations (**Fig. 6a, Sup. Fig. 21**), in agreement with the loss of  
385 endodermal GA-FI in these mutants (**Fig. 3g**)<sup>16</sup> and explaining their loss of suberization (**Fig. 4c, Sup. Fig.**  
386 **7, Sup. Fig. 15-18**). We also considered NPF2.13 which is not expressed in the root (**Fig. 4a**) but contributes  
387 to the long-distance translocation of GA<sub>12</sub> (**Fig. 6a, Sup. Fig. 21**). Reducing long-distance translocation via

388 the *npf2.13* mutation can be simulated by reducing the stele-specific synthesis rate, which leads to reduced  
389 predicted hormone concentrations throughout the root cross-section, again providing an explanation of the  
390 reduction in suberization (**Fig. 4c, Sup. Fig. 15-18**). We concluded that NPF2.12, NPF2.13 and NPF3.1 all  
391 play distinct and necessary roles in creating the hormone accumulation within the endodermis that mediates  
392 suberization.

393 We then used the model to investigate the role of the tonoplast-localized NPF2.14. In contrast to the *npf2.12*,  
394 *npf2.13* and *npf3.1* mutations, simulations of the *npf2.14* mutation predicted endodermal cytoplasmic  
395 hormone concentrations that are higher than those in the wild-type (**Fig. 6a, Sup. Fig. 22**), in agreement  
396 with the GA-FI accumulation at the elongation zone (**Fig. 1i**). Why *npf2.14* exhibits reduced suberization  
397 when endodermal accumulation is higher remained unclear. However, the model predictions revealed that  
398 the vacuolar concentrations in the *npf2.14* pericycle are much lower than in the wild-type (**Fig. 6a. Sup.**  
399 **Fig. 23**). These predictions led us to hypothesize that NPF2.14 regulates hormone levels both inside and  
400 outside of vacuoles which could provide a hormone source in the maturation zone, where the hormone is  
401 no longer supplied by the phloem yet is required for suberization. To test this hypothesis, we simulated the  
402 hormone dynamics after cells leave the phloem unloading zone and found that the presence of NPF2.14  
403 leads to higher predicted endodermal cytoplasmic concentrations as cells mature (**Fig. 6b, Sup. Fig. 24**).  
404 This suggests that the tonoplast-pericycle-localized NPF2.14 ensures that endodermal hormone  
405 concentrations are at levels necessary to mediate suberization. Thus, based on the model, we propose a  
406 pericycle-specific slow-release GA and ABA mechanism that explains how the two hormones are loaded  
407 into the pericycle vacuoles at the phloem unloading zone<sup>41</sup> and released from these vacuoles later on when  
408 the cells are mature (**Fig. 6b**). In this mechanism, GA and ABA unloaded from the phloem are transported  
409 into the pericycle and loaded into the vacuole to form a storage pool. When these cells reach the maturation  
410 zone, the GA and ABA that were stored in the pericycle vacuoles are transported by NPF3 into the  
411 endodermis to induce suberization.

412 In conclusion, the mathematical model revealed that the discovered clade of transporters is sufficient to  
413 explain the observed hormone distributions, with NPF3.1, NPF2.12 and NPF2.13 playing distinct and  
414 necessary roles for endodermal accumulation. Furthermore, the model revealed that the tonoplast-localized  
415 NPF2.14 facilitates vacuolar hormone accumulation within the pericycle which provides a source of  
416 hormone, enabling the cross-section to maintain high endodermal hormone levels after cells leave the  
417 phloem unloading zone<sup>41</sup>. Thus, the model predictions provide mechanistic explanations for the  
418 suberization phenotypes observed in the NPF mutants.

419

## 420 Discussion

421 In this work, we identified *NPF2.14*, a previously uncharacterized transporter, as a dual-specificity GA and  
422 ABA vacuolar transporter. To the best of our knowledge, NPF2.14 is the first known sub-cellular GA/ABA  
423 transporter. We showed that *NPF2.14* is expressed in the pericycle to facilitate endodermal root  
424 suberization. Oocyte experiments showing that NPF2.14 exports GA from the cytosol, combined with  
425 NPF2.14's localization to the tonoplast, indicates that NPF2.14 transports GA and ABA from the cytosol  
426 into the vacuole.

427 The results presented here suggest that the pericycle serves as a buffer zone, regulating the transitions of  
428 hormones from the stele to the endodermis (**Fig. 7**). The stele acts as the source of bioactive GA and ABA  
429 in the root <sup>57,61</sup>. Both hormones have been shown to accumulate and affect their respective response  
430 specifically in the endodermis <sup>25,28,62,63</sup>. In addition, it appears that the GA and ABA do not simply flow  
431 through the pericycle but rather are loaded into the vacuole by NPF2.14 to form a reservoir for later  
432 developmental stages. We propose that the high levels of GA and ABA present in the phloem unloading  
433 zone are taken into the pericycle by NPF2.12. Once in the pericycle cells, NPF2.14 facilitates their import  
434 into the vacuole for storage. We speculate that a slow-release mechanism feeds the differentiating cells with  
435 GA and ABA, thus allowing suberin formation in the mature root (**Fig. 7**). Vacuoles have been proposed  
436 to act as storage, modification, or degradation compartments for plant hormones <sup>64</sup>. It is possible that  
437 tonoplast-localized NPF2.14 mediates the hormonal homeostasis balance that is needed for the proper  
438 execution of the developmental plan in the neighboring cell file. At this point, it is not clear if GA and ABA  
439 are stored at their bioactive form in the vacuole.

440 Confocal imaging of the NLS-YFP lines indicated that both *NPF2.12* and *NPF2.14* are expressed in the  
441 pericycle, mainly at the phloem poles (**Fig. 2a, 4a**). It is therefore possible that the hormone uptake is not  
442 carried out uniformly throughout the pericycle ring, but rather amplified at the pericycle phloem poles cells.  
443 If so, do the two hormones retain polar distribution in the pericycle and in the subsequent endodermis layer?  
444 Or do the hormones have the ability to move within the two cell file rings? Future mathematical models  
445 and genetic work is required to address these questions.

446 The significantly reduced GA<sub>12</sub> content in *npf2.12 npf2.13* double knockout phloem extracts implies that  
447 these transporters are required for GA<sub>12</sub> loading into the phloem and translocation of GA<sub>12</sub> from the shoot  
448 to the root. Thus, we hypothesize that NPF2.12 and NPF2.13, which are plasma membrane-localized  
449 importers expressed in the shoot phloem companion cells, are part of the long-sought mediators of long-  
450 distance GA shoot-to root translocation. Our results are in agreement with the previous finding that GA<sub>12</sub>  
451 is the main form of GA that is transported long distances through the plant <sup>12</sup>. In addition, we showed that



452 GA3ox1 and GA3ox2, which catalyze the final step of active GA production, are expressed in the root stele  
453 <sup>57</sup> (**Fig. 5f**). Thus, once GA<sub>12</sub> docks at the root stele, it is converted by GA3ox1 and GA3ox2 into the  
454 bioactive GA<sub>4</sub> form, which is then delivered from the stele to the endodermis by NPF2.12 and NPF3.1 (**Fig.**  
455 **6c**).

456 It is intriguing that NPF2.12 and NPF2.13 act as GA<sub>12</sub> shoot-to-root transporters and also promote the  
457 delivery of the bioactive forms of GA and ABA to the endodermis. In both cases, a plasma membrane  
458 import activity is involved, but the substrate specificity differs. Since we showed that NPF2.12 and NPF2.13  
459 are able to transport both intermediates of- and the bioactive forms of GA (**Fig. 3b, Sup. Fig. 9-10**) and  
460 that GA<sub>12</sub> is present at high levels in the shoot phloem (**Fig. 5a**), we speculate that GA<sub>12</sub> is the primary  
461 substrate of the transporters. In the root stele, NPF2.12 recognizes bioactive ABA and GA<sub>4</sub>, which are  
462 present in high concentrations due to being synthesized there <sup>61</sup>.

463 The presented work showed for the first time that GA deficiency results in lower endodermal suberization  
464 and can be complemented by GA or ABA. This result is interesting at multiple points of view. First, it may  
465 explain for the first time, the physiological importance of GA accumulation in the endodermis. Second, it  
466 suggests that GA and ABA function non-antagonistically to promote endodermis suberization. At this stage,  
467 it is not clear whether GA promotes endodermis suberization directly by, for example, direct binding and  
468 activation of suberin biosynthesis factors by DELLA or DELLA co-partners, or whether suberization is a  
469 secondary effect of maturation or signaling through the ABA components. Our result in oocytes, suggesting  
470 that GA enhances ABA import, may point to another possibility where the co-activity in regulating suberin  
471 formation at the transport level of the two hormones. While GA and ABA are considered antagonistic  
472 hormones <sup>65</sup>, it is possible that that the two hormones can act non-antagonistically to promote root  
473 suberization by dual-transport activity of the hormones. How does GA promote ABA import biochemically  
474 from the transport structure/function point of view is not clear at the moment. The non-antagonistically  
475 results between the two hormones are in agreement with the growth defects displayed by biosynthesis  
476 mutants of these hormones, which result in small dark green plants <sup>66-68</sup>. Thus, it could be that, in a specific  
477 context where GA and ABA transport plays a role, the two hormones act synergistically.

478

## 479 **Methods**

### 480 **Plant material and growth conditions**

481 All *Arabidopsis thaliana* lines are in a Col-0 background. T-DNA insertion lines were supplied by the  
482 *Arabidopsis* Biological Resource Center. PCR genotyping for homozygous lines was performed using the

483 primers listed in **Sup. Table 1**. To generate *npf2.12 npf2.13* double mutant, *npf2.12* (SALK\_138987) was  
484 crossed to *npf2.13* (SALK\_022429) to obtain an F1 population. F3 homozygous plant was selected by PCR  
485 genotyping. Additional T-DNA lines described in this study: *npf2.12* (SALK\_104042c), and *npf2.13*:  
486 (SALK\_053264). To generate the triple *npf2.12 npf2.13 npf2.14* mutant, a CRISPR/Cas9 construct  
487 targeting *NPF2.14* was introduced into the *npf2.12 npf2.13* double mutant background.

488 Plants were sown on vertical plates containing 0.5 × Murashige-Skoog (MS) medium, 1% sucrose, and  
489 0.8% agar, pH 5.7, stratified for 2 days at 4 °C in the dark, then transferred to growth chambers (Percival  
490 CU41L5) at 21 °C, 100 μE m<sup>-2</sup> s<sup>-1</sup> light intensity under long day light (16 h light/8 h dark). All plants in  
491 suberin quantification experiments were grown on 0.5 × MS medium, 1% sucrose, and 0.8% agar, pH 5.7  
492 for 3 days and subsequently moved to 0.5 × MS medium without sucrose supplementation due to phenotype  
493 masking by the sucrose treatment. For low-nitrate experiments, plants were sown on MS with vitamins,  
494 nitrate free (Caisson labs MSP07-50LT), which was supplemented with 0.01 mM (Low nitrate) or 10 mM  
495 (High nitrate) KNO<sub>3</sub>.

#### 496 **CRISPR**

497 To generate the CRISPR/Cas9 vector targeting *NPF2.14* the MoClo system was implemented. Cloning of  
498 the *NPF2.14* specific guide (Guide sequence: ATTGTTGTCTCGTCGTTAAATCCG) into the system was  
499 done according to Engler et al. <sup>69</sup>.

#### 500 **Hypocotyl cross sections**

501 Sectioning and clearing were performed as describe in Ursache et al <sup>44</sup>. 3-Week-old hypocotyls were fixed  
502 in 4% PFA for an hour, rinsed twice in 1xPBS embedded in 5% agarose and sectioned to 150 μM slices  
503 using a Leica VT1000S vibratome. Slices were cleared using a ClearSee solution for 5 days. Following  
504 clearing sections were counterstained with 0.1% Calcofluor White in ClearSee solution for 30 min. Next,  
505 the seedlings were washed in ClearSee for 30 min with gentle shaking. For imaging, sections were mounted  
506 directly in ClearSee and imaged using a Zeiss LSM 780 inverted microscope.

#### 507 **Hormone application**

508 Hormone was added to the agar medium at concentrations indicated in the figure legends. Seedlings were  
509 either germinated on media or moved after germination to treatment plates. GA-F1 (5 μM) was applied in  
510 liquid MS media for 16 h prior to imaging. For *gal* experiments, both Col-0 and *gal* seeds were imbibed  
511 in sterile water containing 5 μM GA<sub>3</sub> for 16 h to induce uniform germination. Following imbibition, seeds  
512 were washed three times in sterile water to wash away excess GA and were sown on MS plates.

### 513 **Cloning of NPFs overexpression and reporter lines**

514 *NPF2.12* and *NPF2.14* coding sequences were synthesized by Bio Basic Inc., cloned into pENTR/D-TOPO  
515 (Invitrogen K2400), and subsequently cloned into the pH7YWG2 destination vectors using the LR Gateway  
516 reaction (Invitrogen 11791). *NPF2.12* and *NPF2.14* promoters were amplified with the primers listed in  
517 **Sup. Table 2** using a Phusion high-fidelity polymerase (New England Biolabs), cloned into pENTR/D-  
518 TOPO, and then cloned into pMDC7 vector for *NLS-YFP* reporters and pGWB3 vector for GUS reporters.  
519 To generate *pNPF2.13:GUS* reporter, the promoter of *NPF2.13* (1.7-kb fragment) was PCR amplified from  
520 Col-0 genomic DNA with appropriate primers listed in **Sup. Table 2** and inserted into pDONR221  
521 (Invitrogen) by Gateway cloning and recombined with pGWB633<sup>70</sup>.

### 522 **Imaging and analysis**

523 Seedlings were stained in 10 mg/L<sup>-1</sup> propidium iodide (PI) for 5 min, rinsed, and mounted in water.  
524 Seedlings were imaged using a laser scanning confocal microscope (Zeiss LSM 780 inverted microscope),  
525 with argon laser set at 488 nm for fluorescein, 514 nm for YFP, and 561 nm for PI excitation. Emission  
526 filters used were 493-548 nm for fluorescein derivatives, 508-570 nm for YFP, and 583-718 nm for PI  
527 emission. Image analysis and signal quantification were done with the measurement function of ZEN lite  
528 software. The number of quantified biological repeats and sampling points is indicated for each graph in  
529 figure legends.

### 530 **Root length characterization**

531 For root length measurements, seedlings were imaged using Zeiss Stemi 2000-C stereo microscope and  
532 measured using ImageJ software (<http://rsbweb.nih.gov/ij/index.html>).

### 533 **Histochemical GUS staining**

534 Plants were immersed in 100 mM sodium phosphate buffer (pH 7.0) containing 0.1% Triton X-100, 1 mM  
535 5-bromo-4-chloro-3-indolyl- $\beta$ -D-glucuronic acid cyclohexylammonium salt (Sigma-Aldrich), 2 mM  
536 potassium ferricyanide, and 2 mM potassium ferrocyanide. Plants subject to vacuum treatment for 10 min  
537 and then incubated at 37 °C for 16 h. Tissues were cleared with 30%, 50%, and 70% ethanol for 30 min in  
538 each concentration and imaged using an AxioZoom 16, Zeiss binocular microscope.

539 For cross-sectioning of GUS-stained leaf petioles, after clearing in 70% ethanol, the samples were fixed in  
540 FAA solution (3.2% formaldehyde, 5% acetic acid, 50% ethanol) for 30 min and kept overnight at 4°C.  
541 The samples were then dehydrated in an ethanol gradient ranging from 50% to 96%, and incubated in 2%  
542 eosin overnight at 4° C. After several washes in 96% ethanol, the samples were progressively rehydrated

543 in ethanol/HISTO-CLEAR II (Electron Microscopy Sciences) solution, incubated in 50% HISTO-CLEAR  
544 II 50% PARAPLAST PLUS (McCormick Scientific) at 60°C for 2 h, and embedded in 100% PARAPLAST  
545 PLUS. Paraffin-embedded samples were cross-sectioned with LEICA RM2155 microtome and imaged  
546 using a Leica Leitz Dmrb microscope.

#### 547 **Nile red suberin staining, imaging and quantification.**

548 Nile red suberin staining was performed as described by Ursache et al.<sup>44</sup>. In short, 5-day-old seedlings were  
549 fixed in paraformaldehyde for 1 h under gentle agitation and washed twice in phosphate-buffered saline,  
550 pH 7.4. Plants were covered in filtered 0.05% Nile red (Acros Organics, 7385-67-3) solution dissolved in  
551 ClearSee for 16 h. Following staining, plants were washed three times in ClearSee for 30 min each wash.  
552 Next, plants were counterstained with 0.1% calcofluor white (Glenthams Life Sciences, 4404-43-7)  
553 dissolved in ClearSee for cell wall imaging. After 30 min, plants were washed in ClearSee for 30 min.  
554 Plants were mounted directly in ClearSee on slides and imaged with a Zeiss LSM780 confocal microscope.  
555 Images were taken from the upper part of the root and under the root-hypocotyl junction with an argon laser  
556 set at 514 nm for Nile red excitation and 405 nm for calcofluor excitation. Emission filters used were 561-  
557 753 nm filter for Nile red and 410-511 nm filter for calcofluor emission. Fluorescence intensity was  
558 assessed using the Zen software from 5 endodermal cells per root.

559 For root patterning, following Nile red staining, roots were imaged using an AxioZoom 16, Zeiss binocular  
560 microscope. Root length and length of continuously- and patchy-suberized zones was measured using  
561 ImageJ. Percent of suberized area was normalized to total root length.

#### 562 **Quantitative RT-PCR**

563 Total RNA was isolated from the indicated plant materials using RNeasy Plant Mini Kit (QIAGEN 74,904).  
564 DNA was removed by RQ1 RNase-free DNase (Promega M6101). Total RNA (2 µg) converted to  
565 complementary DNA (cDNA) using M-MLV Reverse Transcriptase (Promega M1701) with oligo(dT)15  
566 primer according to manufacturer protocols. Quantitative RT-PCR was performed with 40 ng cDNA in a  
567 final volume of 10 µl with Fast SYBR Green Master Mix (ABI 4385612) using Step One Plus System and  
568 software (ABI). The reaction conditions included 40 amplification cycles, (3 s at 95 °C; 30 s at 60 °C).  
569 Three technical repeats were performed for each cDNA sample, and at least three biological repeats were  
570 used for each treatment. The relative quantification was calculated with the  $\Delta\Delta C_t$  method, PP2A used as  
571 the reference gene. Primers are specified in Supplementary Table 3.

#### 572 **Phylogenetic tree**

573 Protein sequences for *Arabidopsis thaliana* NPF family members were retrieved from TAIR  
574 (<https://www.arabidopsis.org>). Phylogenetic relationships were defined using Phylogeny.fr  
575 (<http://www.phylogeny.fr/>) and visualized with FigTree software  
576 (<http://tree.bio.ed.ac.uk/software/figtree/>).

#### 577 **Transport assays in *Xenopus* oocytes**

578 Coding sequences were cloned into the pNB1u vector, and complementary RNA (cRNA) was produced as  
579 described in Wulff et al. <sup>34</sup>. *Xenopus* oocyte assays were performed as described previously <sup>34</sup>.  
580 Defolliculated *Xenopus laevis* oocytes (stage V-VI) were purchased from Ecocyte Biosciences and were  
581 injected with 25 ng cRNA in 50.6 nl using a Drummond Nanoject II and incubated for 2-4 days at 16 °C in  
582 HEPES-based kulori (90 mM NaCl, 1 mM KCl, 1 mM MgCl<sub>2</sub>, 1 mM CaCl<sub>2</sub>, 5 mM HEPES, pH 7.4) before  
583 use. Oocytes were pre-incubated in MES-based kulori (90 mM NaCl, 1 mM KCl, 1 mM MgCl<sub>2</sub>, 1 mM  
584 CaCl<sub>2</sub>, 5 mM MES, pH 5) for 4 min and were then transferred to phytohormone-containing MES-based  
585 kulori for 60 min. After washing three times in 25 ml HEPES-based kulori followed by one wash in 25 ml  
586 deionized water, oocytes were homogenized in 50% methanol and stored for >30 min at -20 °C. Following  
587 centrifugation (25000 g for 10 min 4 °C), the supernatant was mixed with deionized water to a final  
588 methanol concentration of 20% and filtered through a 0.22-µm filter (MSGVN2250, Merck Millipore)  
589 before analytical LC-MS/MS as described below. For nitrate assays, sodium chloride in kulori was  
590 substituted for equimolar sodium nitrate in order not to affect the membrane potential.

#### 591 **Quantification of phytohormone content by LC-MS/MS**

592 Compounds in the diluted oocyte extracts were directly analyzed by LC-MS/MS. The analysis was  
593 performed with modifications from the method described in Tal et al. <sup>16</sup>. In brief, chromatography was  
594 performed on an Advance UHPLC system (Bruker). Separation was achieved on a Phenomenex Kinetex  
595 1.7u XB-C18 column (100 x 2.1 mm, 1.7 µm, 100 Å) with 0.05% v/v formic acid in water as mobile phase  
596 A and acetonitrile with 0.05% formic acid (v/v) as mobile phase B. The gradients used for elution of GAs  
597 were 0-0.5 min, 2% B; 0.5-1.3 min, 2-30% B; 1.3-2.2 min 30-100% B, 2.2-2.8 min 100% B; 2.8-2.9 min  
598 100-2% B; and 2.9-4.0 min 2% B. The gradients used for elution of ABA were 0-0.5 min, 2% B; 0.5-1.2  
599 min, 2-30% B; 1.2-2.0 min, 30-100% B; 2.0-2.5 min, 100%; 2.5-2.6 min, 100-2% B; and 2.6-4.0 min, 2%  
600 B. The mobile phase flow rate was 400 µl min<sup>-1</sup>, and column temperature was maintained at 40 °C. The  
601 liquid chromatography was coupled to an EVOQ Elite triple quadrupole mass spectrometer (Bruker)  
602 equipped with an electrospray ion source operated in positive and negative ionization mode. Instrument  
603 parameters were optimized by infusion experiments with pure standards. For analysis of GAs, the ion spray  
604 voltage was maintained at +4000 V and -4000 V in positive and negative ionization mode, respectively,

605 and the heated probe temperature was set to 200 °C with probe gas flow at 50 psi. For ABA, the ion spray  
606 voltage was maintained at -3300 V in negative ionization mode, and heated probe temperature was set to  
607 120 °C with probe gas flow at 40 psi. Remaining settings were identical for all analytical methods with  
608 cone temperature set to 350 °C and cone gas to 20 psi. Nebulizing gas was set to 60 psi and collision gas to  
609 1.6 mTorr. Nitrogen was used as probe and nebulizing gas, and argon as collision gas. Active exhaust was  
610 constantly on. Multiple reaction monitoring was used to monitor analyte parent ion to product ion  
611 transitions for all analytes. Multiple reaction monitoring transitions and collision energies were optimized  
612 by direct infusion experiments. Detailed values for mass transitions can be found in **Supplemental Table**  
613 **4**. Both Q1 and Q3 quadrupoles were maintained at unit resolution. Bruker MS Workstation software  
614 (Version 8.2.1) was used for data acquisition and processing. Linearity in ionization efficiencies were  
615 verified by analyzing dilution series of standard mixtures. Sinigrin glucosinolate was used as internal  
616 standard for normalization but not for quantification. Quantification of all compounds was achieved by  
617 external standard curves diluted with the same matrix as the actual samples. All GAs were analyzed together  
618 in a single method. GA<sub>12</sub> suffered from severe ion suppression when combined with the other GAs in the  
619 standard curve, thus quantification was not achieved for GA<sub>12</sub>.

#### 620 **Root suberin monomer profiling by GC-MS**

621 Suberin monomers were extracted from Col-0 and mutant roots according to the protocols previously  
622 described by <sup>71,72</sup>. A sample volume of 1 µL was injected in splitless mode on a GC-MS system (Agilent  
623 7693A Liquid Auto injector, 8860 gas chromatograph, and 5977B mass spectrometer). GC was performed  
624 (HP-5MS UI column; 30 m length, 0.250 mm diameter, and 0.25 µm film thickness; Agilent J&W GC  
625 Columns) with injection temperature of 270°C, interface set to 250°C, and the ion source to 200°C. Helium  
626 was used as the carrier gas at a constant flow rate of 1.2 mL min<sup>-1</sup>. The temperature program was 0.5 min  
627 isothermal at 70°C, followed by a 30°C min<sup>-1</sup> oven temperature ramp to 210°C and a 5°C min<sup>-1</sup> ramp to  
628 330°C, then kept constant during 21 min. Mass spectra were recorded with an *m/z* 40 to 850 scanning range.  
629 Chromatograms and mass spectra were evaluated using the MSD ChemStation software (Agilent).  
630 Integrated peaks of mass fragments were normalized for sample dry weight and the respective C32 alkane  
631 internal standard signal. For identification, the corresponding mass spectra and retention time indices were  
632 compared with the NIST20 library as well as in-house spectral libraries.

#### 633 ***Xenopus* oocyte injection-based efflux transport assays and competition assays.**

634 For injection-based export assays, on the second day of gene expression, oocytes were injected with 23 nl  
635 8.2 mM in 98 mM KCl, 1 mM CaCl<sub>2</sub>, 10 mM HEPES, pH 7.4. T1 oocytes were left 10 min to heal and

636 were then transport was evaluated as described above. T2 oocytes were left for approximately 20 h in  
637 HEPES-based ekulori at 16° C, followed by transport analysis.

### 638 **Quantification of nitrate from oocytes by HPLC**

639 Nitrate concentration in the oocyte extracts was quantified using a Dionex ICS-2100 anion exchange  
640 chromatography system (Thermo Scientific). The separation was done on a Dionex IonPac AG11-HC  
641 analytical column coupled to the AS11-HC guard column (Thermo Scientific). The columns were  
642 connected to a Dionex AERS 500 anion suppressor (Thermo Scientific). The analyses were performed  
643 under the following conditions: sample injection volume 4.8 µl, column temperature 30 °C, flow rate of  
644 0.38 ml/min, isocratic eluent gradient using 30 mM KOH solution in QH<sub>2</sub>O, suppressor current of 29 mA,  
645 and runtime of 15 min. The nitrate detection was done at 220 nm using a Dionex UltiMate 3000 (Thermo  
646 Scientific). QH<sub>2</sub>O water dilutions of Dionex Combined Seven Anion Standard (Thermo Scientific) were  
647 used to create a standard calibration curve. Accuracy and precision of the quantification was checked by  
648 including samples of potassium nitrate throughout the sequence.

### 649 **pH measurements of oocyte lumen**

650 The pH stabilization was performed as described previously<sup>34</sup>. pH-electrodes were pulled from borosilicate  
651 glass capillaries (KWIK-FIL TW F120-3 with filament) on a vertical puller (Narishige Scientific Instrument  
652 Lab), baked for 120 min at 220 °C and silanized for 60 min with dimethyldichlorosilane (Silanization  
653 Solution I, Sigma Aldrich). Electrodes were backfilled with a buffer containing 40 mM KH<sub>2</sub>PO<sub>4</sub>, 23 mM  
654 NaOH and 150 mM NaCl (pH 7.5). The electrode tip was filled with a proton-selective ionophore cocktail  
655 (hydrogen ionophore I cocktail A, Sigma-Aldrich) by dipping the tip into the cocktail. Oocytes, as described  
656 above, were placed in freshly made HEPES-based ekulori (2 mM LaCl<sub>3</sub>, 90 mM NaCl, 1 mM KCl, 1 mM  
657 MgCl<sub>2</sub>, 1 mM CaCl<sub>2</sub>, 5 mM HEPES pH 7.4) for at least 30 min prior to three-electrode voltage clamp  
658 experiments. Before each oocyte a pH calibration curve was made for each oocyte using 100 mM KCl pH  
659 5.5, 100 mM KCl pH 6.5 and 100 mM KCl pH 7.5. Oocytes were clamped at 0 mV and perfused with  
660 HEPES-based ekulori pH 7.4, followed by MES-based ekulori (2 mM LaCl<sub>3</sub>, 90 mM NaCl, 1 mM KCl, 1  
661 mM MgCl<sub>2</sub>, 1 mM CaCl<sub>2</sub>, 5 mM MES pH 5) and internal pH response was measured continuously as a  
662 function of external pH change.

### 663 **Membrane potential measurements**

664 Membrane potentials of oocytes were measured using the automated two-electrode voltage clamp system,  
665 Roboocyte2 (Multi channel systems), in ekulori (90 mM NaCl, 1 mM KCl, 1 mM MgCl<sub>2</sub>, 1 mM CaCl<sub>2</sub>, 5  
666 mM MES, 2 mM LaCl<sub>3</sub>, pH 5) with electrodes backfilled with 1 M KCl and 1.5 M potassium acetate. All

667 oocytes were measured using the same electrodes with a resistance of 280-350 k $\Omega$ . The experiment was  
668 terminated when the resistance of one of the electrodes shifted to approximately 600 k $\Omega$ .

### 669 **Two-electrode voltage clamp electrophysiology**

670 The electric signal elicited by GA treatment of oocytes was measured using the automated two-electrode  
671 voltage clamp system Robocyte2 (Multi channel systems), in ekulori (90 mM NaCl, 1 mM KCl, 1 mM  
672 MgCl<sub>2</sub>, 1 mM CaCl<sub>2</sub>, 5 mM MES, 2 mM LaCl<sub>3</sub> pH 4.5 or pH 5) with electrodes (resistance 280-1000 k $\Omega$ )  
673 backfilled with 1 M KCl and 1.5 M potassium acetate. Oocytes were clamped at – 60 mV, and IV curves  
674 were obtained before and after substrate addition. Substrate dependent currents were calculated by  
675 subtracting currents before addition of substrate from currents after addition of substrate.

### 676 **Root hormone quantification**

677 Hormone extraction and analysis was performed as described in Zhang et al., 2021. Standards (both  
678 labelled and non-labelled) were obtained from Olchemim Ltd. (Olomouc, Czech Republic) and  
679 National Research Council (NRC-CNRC, Canada). Standard grade solvents were used for sample  
680 preparation, Methanol, Acetic acid (LiChrosolv, Sigma-Aldrich, USA), Acetonitrile (J.T.Baker,  
681 Avantor, PA, USA), Formic acid (Honeywell Fluka, Thermo Fisher Scientific, MA, USA) and de-  
682 ionized water (Milli-Q, Synergy-UV millipore system, USA). Briefly, root tissue frozen in liquid  
683 nitrogen was grounded using motor and pestle. Around 200 mg of root sample was measured from ground  
684 powder and extracted with ice cold methanol/water/formic acid (15/4/1 v/v/v) added with deuterium  
685 labelled internal standards (IS). Similar concentrations of IS of abscisic acid and gibberellin (GA<sub>4</sub>) were  
686 added into samples and calibration standards. The samples were purified using Oasis MCX SPE  
687 cartridges (Waters, USA) according to manufacturer's protocol. The samples were injected on  
688 Acquity UPLC BEH C18 column (1.7  $\mu$ m, 2.1x100 mm, Waters; with gradients of 0.1% acetic  
689 acid in water or acetonitrile), connected to Acquity UPLC H class system (with Waters Acquity  
690 QSM, FNR sample manager and PDA) coupled with UPLC-ESI-MS/MS triple quadrupole mass  
691 spectrometer (Xevo TQ-S, Waters, equipped with ESI probe) for identification and quantification  
692 of hormones. The hormones were measured using MS detector, both in positive and negative  
693 mode, with two MRM transitions for each compound. External calibration curves were constructed  
694 with hormone standards added with IS, used for quantification, and calculated through Target Lynx (v4.1;  
695 Waters) software by comparing the ratios of MRM peak areas of analyte to that of internal standard.

### 696 **Phloem extract and hormone quantification**



697 Rosette leaves of 5-week-old Col-0 and *npf2-12 npf2-13* mutant plants (before bolting) were cut with a  
698 razor blade at the base of the petiole, and each leaf was dipped in a tube containing 80  $\mu$ L of exudation  
699 buffer (50 mM potassium phosphate buffer, pH7.6, 10 mM EDTA). Exudation was carried out for 3h in  
700 dark in high humidity to limit transpiration. Exudation of 75 leaves was regrouped and concentrated under  
701 vacuum centrifugation. Hormone contents in phloem exudates were determined by UPLC system-MS/MS  
702 (Waters Quattro Premier XE). Concentrated residue of phloem sap was resuspended with 80% methanol-  
703 1% acetic acid including  $17\text{-}^2\text{H}_2$ -labeled GA internal standards (Olchemim), mixed and passed through an  
704 Oasis HLB column. The dried eluate was dissolved in 5% acetonitrile-1% acetic acid, and the GAs were  
705 separated by UPHL chromatography (Accucore RP-MS column 2.6  $\mu$ m, 100 x 2.1 mm; ThermoFisher  
706 Scientific) with a 5 to 50% acetonitrile gradient containing 0.05% acetic acid, at 400  $\mu$ L/min over 22 min.  
707 The concentrations of GAs in the extracts were analyzed with a Q-Exactive mass spectrometer (Orbitrap  
708 detector; ThermoFisher Scientific) by targeted SIM using embedded calibration curves and the Xcalibur  
709 2.2 SP1 build 48 and TraceFinder programs.

#### 710 **Grafting assays.**

711 Grafting was performed without collars on water imbibed 0.45  $\mu$ M MCE membrane (Millipore) between  
712 hypocotyls of rootstocks and scions of 6-day-old seedlings grown on 1x MS agar plate. Grafted seedlings  
713 were then kept vertically to recover, for 5 days under constant humidity. Successful grafts were transferred  
714 onto  $\frac{1}{2}$ x MS agar plates and grown under a 16h photoperiod at 22°C. Root growth was measured every day  
715 for 3 days with ImageJ (<https://imagej.nih.gov/ij/download.html>). Nile red suberin staining fluorescence  
716 intensity was assessed as previously described, in roots of 13-day-old grafted seedlings, two days after  
717 transfer onto  $\frac{1}{2}$ x MS agar plates.

#### 718 **DELLA degradation assays.**

719 12-day-old seedlings were transferred to 1x MS agar modified medium without nitrogen (bioWORLD plant  
720 media) supplemented with 0.5 mM  $\text{KNO}_3$  and 1  $\mu$ M paclobutrazol (Sigma). 4 days after transfer, a drop of  
721  $\text{GA}_{12}$  (5  $\mu$ l at 1  $\mu$ M) was placed on one of the first two leaves formed. Roots were collected 6, 12 and 24h  
722 after adding  $\text{GA}_{12}$ . Total proteins were extracted in 2x SDS-PAGE sample buffer and separated on 10%  
723 SDS-PAGE gel. After transfer onto membrane, immunoblots were performed using a 2000-fold dilution  
724 anti-RGA (Agrisera) and a 10000-fold dilution of peroxidase-conjugated goat anti-rabbit (Thermo Fisher  
725 Scientific). Signals were detected with Fusion FX (Vilber) using Immobilon Forte Western HRP Substrate  
726 (Millipore). The blot was subsequently stained with Coomassie blue. Quantification of the signals was  
727 determined using ImageJ package.

#### 728 **Mathematical model.**

729 Root templates were segmented from an experimental image using the CellSeT image analysis tool <sup>73</sup> (**Sup.**  
730 **Fig. 20**). We used CellSeT to manually assign a cell type to each cell and then read the geometrical and  
731 cell-type data into a tissue database (based on the OpenAlea tissue structure <sup>74</sup>), extending the data structure  
732 to incorporate vacuolar compartments within each cell. The geometrical, topological and transporter-  
733 distribution data were used to form a system of ordinary differential equations (ODEs) to describe the GA  
734 transport, synthesis and degradation within the multicellular root cross-section. Parameters associated with  
735 the passive and transporter-mediated transport components were estimated using the oocyte data (**Fig. 1a**,  
736 **Fig. 3b**) and the remaining parameter values were obtained from the literature (**Sup. Table 5**). These ODEs  
737 were simulated using the `solve_ivp` package in python 3.6.5. Full details of the model equations and  
738 assumptions are provided as Supplementary text.

739

#### 740 **Acknowledgments**

741 We thank Daria Binenbaum for the illustrations and Peter Hedden (Rothamsted Research) for sharing  
742 *pGA3ox1-4:GUS* seeds. Funding: This work was supported by grants from the Israel Science Foundation  
743 (2378/19 and 3419/20 to E.S.), the Human Frontier Science Program (HFSP—RGY0075/2015 and HFSP—  
744 LIY000540/2020 to E.S., H.H.N.-E. and L.R.B.), Danmarks Grundforskningsfond (DNRF99 to H.H.N.-  
745 E.), the European Research Council (757683-RobustHormoneTrans to E.S.), the Constantiner Travel  
746 Fellowship (to J.B.), the Centre National de la Recherche Scientifique (to L.S-A. J-M.D. and P.A.), the  
747 French Ministry of Research and Higher Education studentship (to L.C.).

748

#### 749 **Author contributions**

750 J.B. performed the research and wrote the manuscript. N.W. performed the oocyte transporter assays. L.C.,  
751 L.S-A., J-M.D. and P.A carried out long-distance transport assays. K.K. performed the mathematical  
752 modelling. I.T. assisted in cloning overexpression and reporter lines. H.V. and A.A. quantified root GA and  
753 ABA content. M.A. helped with genotyping T-DNA mutant lines and profiling suberin patterning. Y.Z.  
754 helped with *npf* mutant identification. D.R. and L.R. assisted in cross sectioning and staining. E.C.  
755 quantified hormone content in the phloem sap. E.M. and H.C. performed suberin monomer quantifications.  
756 S.L. and R.W. synthesized fluorescently tagged hormones. S.B carried the qPCR and hormones treated  
757 reporter lines. V.N. and C.C. helped with nitrate and hormones quantification in oocyte assays, respectively.  
758 C. H carried out hormone competition transport assays. L.B., P.A., H.H.N.-E. and ES designed and  
759 supervised the work and edited the manuscript. All authors discussed the results and commented on the  
760 manuscript.

761

762 **Competing interests:** The authors declare that they have no competing interests.

763

764 **Data and materials availability:** All the data supporting the findings of this study are available within  
765 the article and the Supplementary Materials.

766

## 767 **References**

- 768 1. Hedden, P. & Sponsel, V. A Century of Gibberellin Research. *Journal of Plant Growth Regulation*  
769 *2015 34:4 34*, 740–760 (2015).
- 770 2. Eriksson, S., Böhlenius, H., Moritz, T. & Nilsson, O. GA4 Is the Active Gibberellin in the Regulation  
771 of LEAFY Transcription and Arabidopsis Floral Initiation. *Plant Cell* **18**, 2172–2181 (2006).
- 772 3. Proebsting, W. M., Hedden, P., Lewis, M. J., Croker, S. J. & Proebsting, L. N. Gibberellin  
773 Concentration and Transport in Genetic Lines of Pea Effects of Grafting. *Plant Physiol* **100**, 1354–  
774 1360 (1992).
- 775 4. Björklund, S., Antti, H., Uddestrand, I., Moritz, T. & Sundberg, B. Cross-talk between gibberellin  
776 and auxin in development of Populus wood: gibberellin stimulates polar auxin transport and has  
777 a common transcriptome with auxin. *The Plant Journal* **52**, 499–511 (2007).
- 778 5. Dayan, J. *et al.* Leaf-Induced Gibberellin Signaling Is Essential for Internode Elongation, Cambial  
779 Activity, and Fiber Differentiation in Tobacco Stems. *Plant Cell* **24**, 66–79 (2012).
- 780 6. Chin, T. Y. & Lockhart, J. A. TRANSLOCATION OF APPLIED GIBBERELLIN IN BEAN SEEDLINGS. *Am J*  
781 *Bot* **52**, 828–833 (1965).
- 782 7. ZWEIG, G., YAMAGUCHI, S. & MASON, G. W. Translocation of C 14 -Gibberellin in Red Kidney  
783 Bean, Normal Corn, and Dwarf Corn . 122–134 (1961) doi:10.1021/BA-1961-0028.CH013.
- 784 8. Hoad, G. v. & Bowen, M. R. Evidence for gibberellin-like substances in phloem exudate of higher  
785 plants. *Planta* **82**, 22–32 (1968).
- 786 9. Hu, J. *et al.* Potential Sites of Bioactive Gibberellin Production during Reproductive Growth in  
787 Arabidopsis. *Plant Cell* **20**, 320–336 (2008).
- 788 10. Weiss, D. & Halevy, A. H. Stamens and gibberellin in the regulation of corolla pigmentation and  
789 growth in *Petunia hybrida*. *Planta* *1989 179:1 179*, 89–96 (1989).
- 790 11. Hedden, P. & Thomas, S. G. Gibberellin biosynthesis and its regulation. *Biochemical Journal* **444**,  
791 11–25 (2012).
- 792 12. Regnault, T. *et al.* The gibberellin precursor GA12 acts as a long-distance growth signal in  
793 Arabidopsis. *Nature Plants* *2015 1:6 1*, 1–6 (2015).
- 794 13. Camut, L. *et al.* Root-derived GA12 contributes to temperature-induced shoot growth in  
795 Arabidopsis. *Nature Plants* *2019 5:12 5*, 1216–1221 (2019).

- 796 14. Chiba, Y. *et al.* Identification of *Arabidopsis thaliana* NRT1/PTR FAMILY (NPF) proteins capable of  
797 transporting plant hormones. *Journal of Plant Research* 2015 128:4 **128**, 679–686 (2015).
- 798 15. Kanno, Y. *et al.* AtSWEET13 and AtSWEET14 regulate gibberellin-mediated physiological  
799 processes. *Nature Communications* 2016 7:1 **7**, 1–11 (2016).
- 800 16. Tal, I. *et al.* The *Arabidopsis* NPF3 protein is a GA transporter. *Nature Communications* 2016 7:1  
801 **7**, 1–11 (2016).
- 802 17. Saito, H. *et al.* The jasmonate-responsive GTR1 transporter is required for gibberellin-mediated  
803 stamen development in *Arabidopsis*. *Nature Communications* 2015 6:1 **6**, 1–11 (2015).
- 804 18. Corratgé-Faillie, C. & Lacombe, B. Substrate (un)specificity of *Arabidopsis* NRT1/PTR FAMILY  
805 (NPF) proteins. *J Exp Bot* **68**, 3107–3113 (2017).
- 806 19. Nour-Eldin, H. H. *et al.* NRT/PTR transporters are essential for translocation of glucosinolate  
807 defence compounds to seeds. *Nature* 2012 488:7412 **488**, 531–534 (2012).
- 808 20. Kramer, E. M. How Far Can a Molecule of Weak Acid Travel in the Apoplast or Xylem? *Plant*  
809 *Physiol* **141**, 1233–1236 (2006).
- 810 21. Binenbaum, J., Weinstain, R. & Shani, E. Gibberellin Localization and Transport in Plants. *Trends*  
811 *Plant Sci* **23**, 410–421 (2018).
- 812 22. Zhu, J. K. Abiotic Stress Signaling and Responses in Plants. *Cell* **167**, 313–324 (2016).
- 813 23. Cutler, S. R., Rodriguez, P. L., Finkelstein, R. R. & Abrams, S. R. Abscisic Acid: Emergence of a Core  
814 Signaling Network. <https://doi.org/10.1146/annurev-arplant-042809-112122> **61**, 651–679 (2010).
- 815 24. Liu, X. & Hou, X. Antagonistic regulation of ABA and GA in metabolism and signaling pathways.  
816 *Front Plant Sci* **9**, 251 (2018).
- 817 25. Ubeda-Tomás, S. *et al.* Root growth in *Arabidopsis* requires gibberellin/DELLA signalling in the  
818 endodermis. *Nature Cell Biology* 2008 10:5 **10**, 625–628 (2008).
- 819 26. Ubeda-Tomás, S. *et al.* Gibberellin Signaling in the Endodermis Controls *Arabidopsis* Root  
820 Meristem Size. *Current Biology* **19**, 1194–1199 (2009).
- 821 27. Duan, L. *et al.* Endodermal ABA Signaling Promotes Lateral Root Quiescence during Salt Stress in  
822 *Arabidopsis* Seedlings. *Plant Cell* **25**, 324–341 (2013).
- 823 28. Shani, E. *et al.* Gibberellins accumulate in the elongating endodermal cells of *Arabidopsis* root.  
824 *Proceedings of the National Academy of Sciences* **110**, 4834–4839 (2013).
- 825 29. David, L. C. *et al.* N availability modulates the role of NPF3.1, a gibberellin transporter, in GA-  
826 mediated phenotypes in *Arabidopsis*. *Planta* **244**, 1315–1328 (2016).
- 827 30. Andersen, T. G., Barberon, M. & Geldner, N. Suberization — the second life of an endodermal  
828 cell. *Curr Opin Plant Biol* **28**, 9–15 (2015).
- 829 31. Shukla, V. & Barberon, M. Building and breaking of a barrier: Suberin plasticity and function in  
830 the endodermis. *Curr Opin Plant Biol* **64**, 102153 (2021).

- 831 32. Barberon, M. The endodermis as a checkpoint for nutrients. *New Phytologist* **213**, 1604–1610  
832 (2017).
- 833 33. Zhang, Y. *et al.* ABA homeostasis and long-distance translocation are redundantly regulated by  
834 ABCG ABA importers. *Sci Adv* **7**, (2021).
- 835 34. Wulff, N. *et al.* An Optimized Screen Reduces the Number of GA Transporters and Provides  
836 Insights Into Nitrate Transporter 1/Peptide Transporter Family Substrate Determinants. *Front*  
837 *Plant Sci* **0**, 1106 (2019).
- 838 35. Jørgensen, M. E. *et al.* A Functional EXXEK Motif is Essential for Proton Coupling and Active  
839 Glucosinolate Transport by NPF2.11. *Plant Cell Physiol* **56**, 2340–2350 (2015).
- 840 36. Solcan, N. *et al.* Alternating access mechanism in the POT family of oligopeptide transporters.  
841 *EMBO J* **31**, 3411–3421 (2012).
- 842 37. Tsay, Y. F., Schroeder, J. I., Feldmann, K. A. & Crawford, N. M. The herbicide sensitivity gene CHL1  
843 of arabidopsis encodes a nitrate-inducible nitrate transporter. *Cell* **72**, 705–713 (1993).
- 844 38. Campilho, A., Nieminen, K. & Ragni, L. The development of the periderm: the final frontier  
845 between a plant and its environment. *Curr Opin Plant Biol* **53**, 10–14 (2020).
- 846 39. Beeckman, T., Burssens, S. & Inzé, D. The peri-cell-cycle in Arabidopsis. *J Exp Bot* **52**, 403–411  
847 (2001).
- 848 40. Takano, J. *et al.* Arabidopsis boron transporter for xylem loading. *Nature* **2002 420:6913 420**,  
849 337–340 (2002).
- 850 41. Ross-Elliott, T. J. *et al.* Phloem unloading in arabidopsis roots is convective and regulated by the  
851 phloempole pericycle. *Elife* **6**, (2017).
- 852 42. Wunderling, A. *et al.* A molecular framework to study periderm formation in Arabidopsis. *New*  
853 *Phytologist* **219**, 216–229 (2018).
- 854 43. Barberon, M. *et al.* Adaptation of Root Function by Nutrient-Induced Plasticity of Endodermal  
855 Differentiation. *Cell* **164**, 447–459 (2016).
- 856 44. Ursache, R., Andersen, T. G., Marhavý, P. & Geldner, N. A protocol for combining fluorescent  
857 proteins with histological stains for diverse cell wall components. *The Plant Journal* **93**, 399–412  
858 (2018).
- 859 45. Lux, A., Morita, S., Abe, J. & Ito, K. An Improved Method for Clearing and Staining Free-hand  
860 Sections and Whole-mount Samples. *Ann Bot* **96**, 989–996 (2005).
- 861 46. Kreszies, T., Schreiber, L. & Ranathunge, K. Suberized transport barriers in Arabidopsis, barley  
862 and rice roots: From the model plant to crop species. *J Plant Physiol* **227**, 75–83 (2018).
- 863 47. Woolfson, K. N., Esfandiari, M. & Bernards, M. A. Suberin Biosynthesis, Assembly, and Regulation.  
864 *Plants* **2022, Vol. 11, Page 555 11**, 555 (2022).

- 865 48. Barberon, M. *et al.* Adaptation of Root Function by Nutrient-Induced Plasticity of Endodermal  
866 Differentiation. *Cell* **164**, 447–459 (2016).
- 867 49. Aloni, R. Vascular Differentiation and Plant Hormones. *Vascular Differentiation and Plant*  
868 *Hormones* (2021) doi:10.1007/978-3-030-53202-4.
- 869 50. Wang, C. *et al.* Developmental programs interact with abscisic acid to coordinate root  
870 suberization in Arabidopsis. *The Plant Journal* **104**, 241–251 (2020).
- 871 51. Sunai', T.-P. & Kamiya, Y. The Arabidopsis GA1 locus encodes the cyclase ent-kaurene synthetase  
872 A of gibberellin biosynthesis. *Plant Cell* **6**, 1509–1518 (1994).
- 873 52. Lin, Q. *et al.* The SnRK2-APC/CTE regulatory module mediates the antagonistic action of  
874 gibberellic acid and abscisic acid pathways. *Nature Communications* **2015 6:1** **6**, 1–10 (2015).
- 875 53. Almagro, A., Lin, S. H. & Tsay, Y. F. Characterization of the Arabidopsis Nitrate Transporter NRT1.6  
876 Reveals a Role of Nitrate in Early Embryo Development. *Plant Cell* **20**, 3289–3299 (2009).
- 877 54. Fan, S. C., Lin, C. S., Hsu, P. K., Lin, S. H. & Tsay, Y. F. The Arabidopsis Nitrate Transporter NRT1.7,  
878 Expressed in Phloem, Is Responsible for Source-to-Sink Remobilization of Nitrate. *Plant Cell* **21**,  
879 2750–2761 (2009).
- 880 55. Regnault, T. *et al.* The gibberellin precursor GA12 acts as a long-distance growth signal in  
881 Arabidopsis. *Nature Plants* **2015 1:6** **1**, 1–6 (2015).
- 882 56. Sun, T. P. The Molecular Mechanism and Evolution of the GA–GID1–DELLA Signaling Module in  
883 Plants. *Current Biology* **21**, R338–R345 (2011).
- 884 57. Barker, R. *et al.* Mapping sites of gibberellin biosynthesis in the Arabidopsis root tip. *New*  
885 *Phytologist* **229**, 1521–1534 (2021).
- 886 58. Band, L. R. *et al.* Systems Analysis of Auxin Transport in the Arabidopsis Root Apex. *Plant Cell* **26**,  
887 862–875 (2014).
- 888 59. Mathieu, Y. *et al.* Regulation of Vacuolar pH of Plant Cells I. Isolation and Properties of Vacuoles  
889 Suitable for <sup>31</sup>P NMR Studies. *Plant Physiol* **89**, 19–26 (1989).
- 890 60. Hedrich, R., Mueller, T. D., Becker, D. & Marten, I. Structure and Function of TPC1 Vacuole SV  
891 Channel Gains Shape. *Mol Plant* **11**, 764–775 (2018).
- 892 61. Kuromori, T., Sugimoto, E. & Shinozaki, K. Intertissue Signal Transfer of Abscisic Acid from  
893 Vascular Cells to Guard Cells. *Plant Physiol* **164**, 1587–1592 (2014).
- 894 62. De Diego, N. *et al.* Immunolocalization of IAA and ABA in roots and needles of radiata pine (*Pinus*  
895 *radiata*) during drought and rewatering. *Tree Physiol* **33**, 537–549 (2013).
- 896 63. Ondzighi-Assoume, C. A., Chakraborty, S. & Harris, J. M. Environmental Nitrate Stimulates  
897 Abscisic Acid Accumulation in Arabidopsis Root Tips by Releasing It from Inactive Stores. *Plant*  
898 *Cell* **28**, 729–745 (2016).

- 899 64. Martinoia, E., Meyer, S., De Angeli, A. & Nagy, R. Vacuolar transporters in their physiological  
900 context. *Annu Rev Plant Biol* **63**, 183–213 (2012).
- 901 65. Shu, K., Zhou, W., Chen, F., Luo, X. & Yang, W. Abscisic acid and gibberellins antagonistically  
902 mediate plant development and abiotic stress responses. *Front Plant Sci* **9**, 416 (2018).
- 903 66. Peng, J. & Harberd, N. P. Gibberellin Deficiency and Response Mutations Suppress the Stem  
904 Elongation Phenotype of Phytochrome-Deficient Mutants of Arabidopsis'. *Plant Physiol* **113**  
905 (1997).
- 906 67. González-Guzmán, M. *et al.* The Short-Chain Alcohol Dehydrogenase ABA2 Catalyzes the  
907 Conversion of Xanthoxin to Abscisic Aldehyde. *Plant Cell* **14**, 1833–1846 (2002).
- 908 68. Merilo, E. *et al.* Stomatal VPD Response: There Is More to the Story Than ABA. *Plant Physiol* **176**,  
909 851 (2018).
- 910 69. Engler, C. *et al.* A Golden Gate Modular Cloning Toolbox for Plants. (2014)  
911 doi:10.1021/sb4001504.
- 912 70. Nakamura, S. *et al.* Gateway Binary Vectors with the Bialaphos Resistance Gene, bar, as a  
913 Selection Marker for Plant Transformation. *OUP* **74**, 1315–1319 (2014).
- 914 71. Cohen, H. *et al.* A Multilevel Study of Melon Fruit Reticulation Provides Insight into Skin Ligno-  
915 Suberization Hallmarks. *Plant Physiol* **179**, 1486–1501 (2019).
- 916 72. Cohen, H., Fedyuk, V., Wang, C., Wu, S. & Aharoni, A. SUBERMAN regulates developmental  
917 suberization of the Arabidopsis root endodermis. *The Plant Journal* **102**, 431–447 (2020).
- 918 73. Pound, M. P., French, A. P., Wells, D. M., Bennett, M. J. & Pridmore, T. P. CellSeT: Novel  
919 Software to Extract and Analyze Structured Networks of Plant Cells from Confocal Images. *Plant*  
920 *Cell* **24**, 1353 (2012).
- 921 74. Pradal, C. *et al.* OpenAlea: a visual programming and component-based software platform for  
922 plant modelling. *Functional Plant Biology* **35**, 751–760 (2008).
- 923

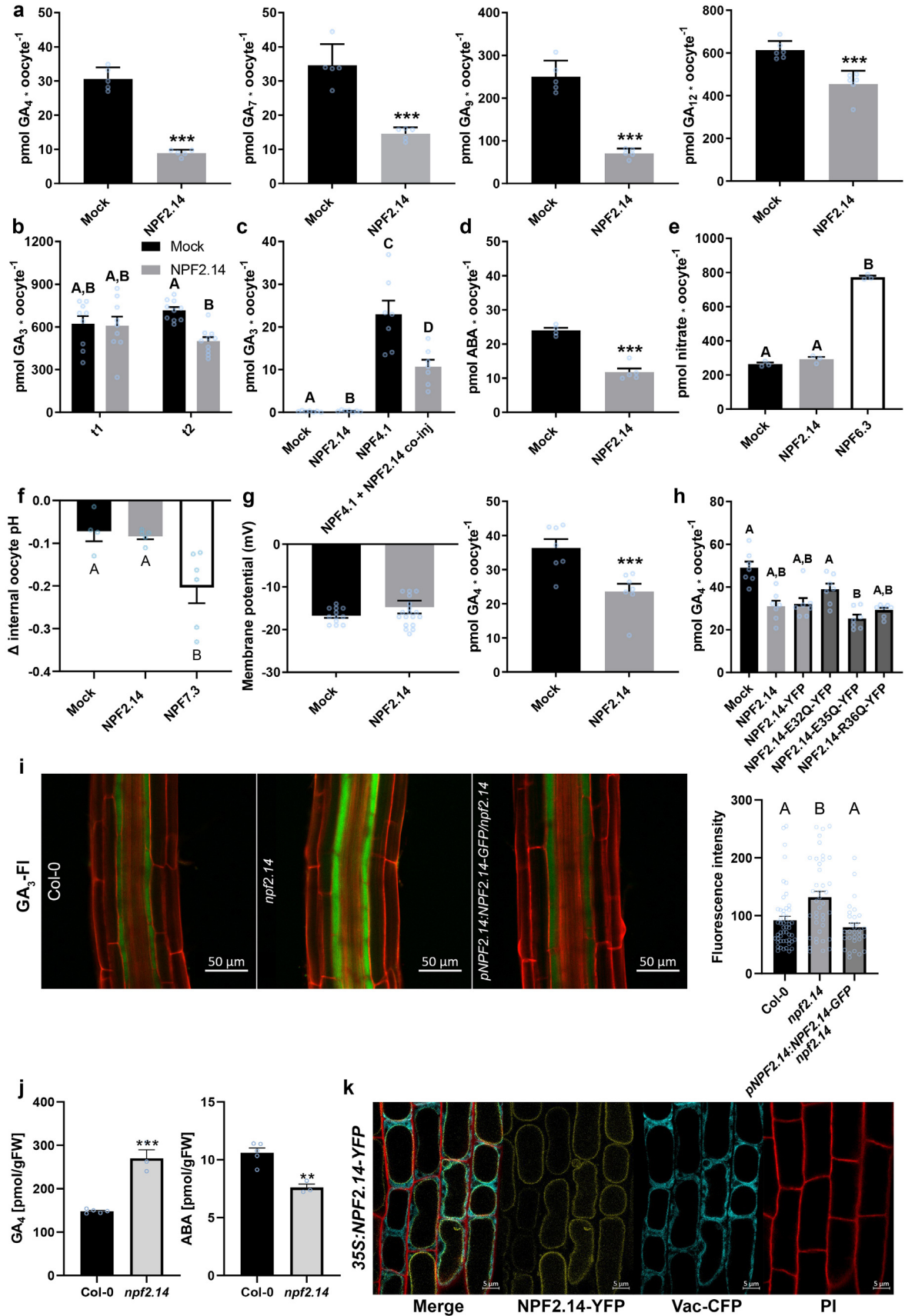




**Fig. 1. NPF2.14 is a vacuolar GA and ABA transporter.** (a) GA accumulation in NPF2.14-expressing and control oocytes exposed to the indicated GAs at 50  $\mu$ M concentration for 60 min at room temperature at pH 5 for GA<sub>4</sub> and GA<sub>7</sub> and at pH 6 for GA<sub>9</sub> and GA<sub>12</sub> (n = 5 for GA<sub>4</sub>, GA<sub>7</sub>, and GA<sub>9</sub> and n = 6 for GA<sub>12</sub>). Statistical significance was evaluated by two-tailed t-tests ( $p \leq 0.05$ ). (b) GA accumulation at 20 h after direct injection of 23 nl of 8.2 mM membrane impermeable GA<sub>3</sub> at pH 7.4 at 16° C (t1) and after 60 min at room temperature at pH 5 (t2) (n = 6). Statistical significance was determined by Holm Sidak two-way ANOVA ( $p \leq 0.05$ ). (c) GA accumulation in control oocytes or oocytes that express NPF2.14, NPF4.1, or both proteins exposed to 50  $\mu$ M GA<sub>3</sub> at pH 5 for 60 min at room temperature and analyzed by LC-MS/MS (n = 7). Statistical significance was assessed using a Holm Sidak one-way ANOVA ( $p = 0.05$ ). (d) ABA accumulation in oocytes exposed to 50  $\mu$ M ABA at pH 5 for 60 min at room temperature (n = 5). Statistical significance was determined by two-tailed t-test ( $p = 0.05$ ). (e) Nitrate accumulation in oocytes exposed to 5 mM nitrate at pH 5 at room temperature for 60 min (three replicates of 5 oocytes analyzed by analytical anion chromatography). Statistical significance was assessed using a Holm Sidak one-way ANOVA ( $p = 0.05$ ). (f) Internal oocyte pH measured using three-electrode voltage clamp electrophysiology of control oocytes and NPF2.14- and NPF7.3-expressing oocytes. Oocytes were perfused at pH 7.4 for 5 min followed by perfusion at pH 5 for 5 min (n = 4-6 single oocytes). Statistical significance was assessed using Holm Sidak one-way ANOVA ( $p = 0.05$ ). (g) Membrane potentials of control oocytes (n = 12) and NPF2.14-expressing oocytes (n = 19) measured at pH 5 using two-electrode voltage clamp electrophysiology. Oocytes with measured membrane potential were exposed to 50  $\mu$ M GA<sub>4</sub> at pH 5 (n = 7 single oocytes) for 60 min at room temperature and analyzed by LC-MS/MS. Statistical significance was assessed using two-tailed t-tests ( $***p < 0.001$ ). (h) GA accumulation in control oocytes or oocytes that express NPF2.14 with wild-type or mutant ExxE[K/R] motifs exposed to 50  $\mu$ M GA<sub>4</sub> at pH 5 for 60 min at room temperature and analyzed by LC-MS/MS (n = 7). Statistical significance was assessed using a Holm Sidak one-way ANOVA ( $p = 0.05$ ). (i) Left: Representative images of 6-day-old *npf2.14* mutant and *npf2.14* complementation lines. Roots were treated with 5  $\mu$ M GA<sub>3</sub>-Fl (green); propidium iodide (red). Right: GA<sub>3</sub>-Fl fluorescence intensity in the endodermis, mean  $\pm$  S.E (5 endodermal cells sampled from a minimum of 7 biological repeats, n > 35). (j) GA<sub>4</sub> and ABA content in 10-day-old roots of control and *npf2.14*-mutant plants measured using LC-MS. n = 5. Significance was evaluated using a Student's t-test ( $**p < 0.01$ ,  $***p \leq 0.0001$ ). (k) Representative confocal image of 6-day-old root epidermis *35S:NPF2.14-YFP* cells stained with propidium iodide (red) and tonoplast marker Vac-CFP (cyan)<sup>1</sup>.

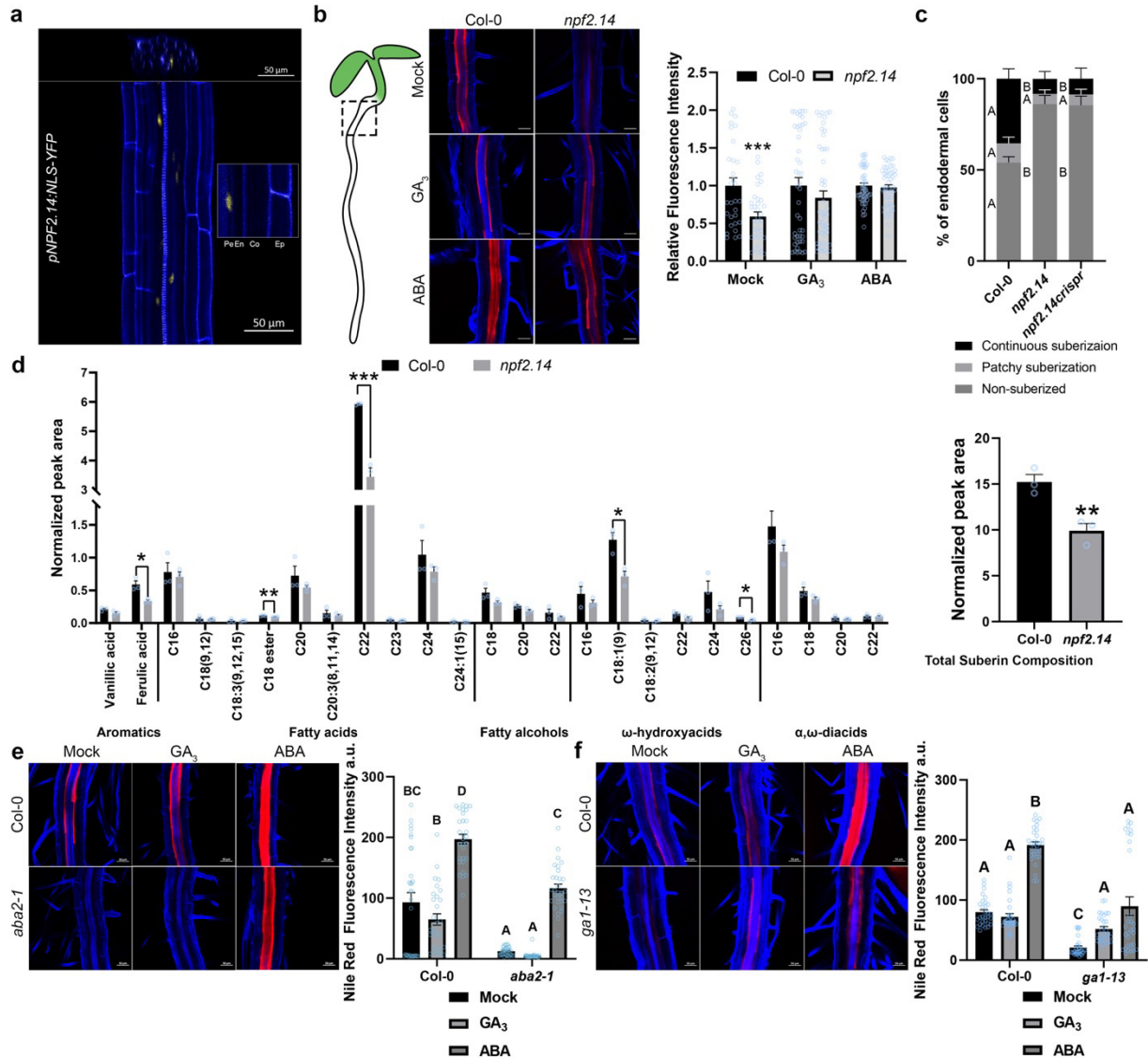


**Fig. 2. *NPF2.14* expression in the differentiated pericycle is required for endodermal root suberization.** (a) Confocal image of 6-day-old *pNPF2.14:NLS-YFP* roots stained with propidium iodide (blue) and imaged for YFP (yellow). Inset is magnification of cells with *pNPF2.14:NLS-YFP* signal. Pe – Pericycle, En - Endodermis, Co – Cortex, Ep – Epidermis. (b) Left: Images of 5-day-old Col-0 and *npf2.14* mutant roots supplemented with mock solution, 5  $\mu$ M GA<sub>3</sub> or 1  $\mu$ M ABA and stained with Nile red (red) and calcofluor (blue). Right: Quantification of Nile red fluorescence intensity was normalized to Col-0 for each treatment. Illustration indicates imaged area. Fluorescent intensity was quantified from a minimum of 10 roots per treatment, 5 endodermal cells per root,  $n > 50$ . Statistical significance was assessed using a Dunnett's test (\*\*\*)  $p < 0.001$ . (c) Quantifications of suberin pattern along the root using Nile red fluorescence intensity,  $n = 10$ . Different letters indicate significant differences between conditions ( $p < 0.05$ ). (d) Root suberin profile for 10-day-old plants, measured by gas chromatography-mass spectrometry. The y-axis represents relative peak areas following normalization to a C<sub>32</sub>-alkane internal standard. Right graph indicates for total suberin composition. Data in bars represent the means  $\pm$  SE of three biological replicates. \* indicates statistically significant differences compared with Col-0 at  $p \leq 0.05$ , \*\*  $p \leq 0.01$  and \*\*\*  $p \leq 0.001$  by Student's t-test. (e) Left: Images of 5-day-old Col-0 and *aba2-1* roots from plants grown on mock MS or MS with 1  $\mu$ M ABA. Roots were stained with Nile red (red) and calcofluor (blue). Right:

Fluorescent intensity was quantified from a minimum of 10 roots per treatment, 5 endodermal cells per root,  $n > 50$ . Significance was determined using Tukey's ad-hoc statistical test (treatments marked with different letters are significantly different). (f) Left: Images of 5-day-old Col-0 and *gal-13* mutant roots from plants grown on mock MS or MS with 5  $\mu$ M GA<sub>3</sub>. Roots were stained with Nile red (red) and calcofluor (blue). Right: Fluorescent intensity was quantified from a minimum of 8 roots per treatment, 5 endodermal cells per root,  $n > 40$ . Significance was determined using Tukey's ad-hoc statistical test (treatments marked with different letters are significantly different).

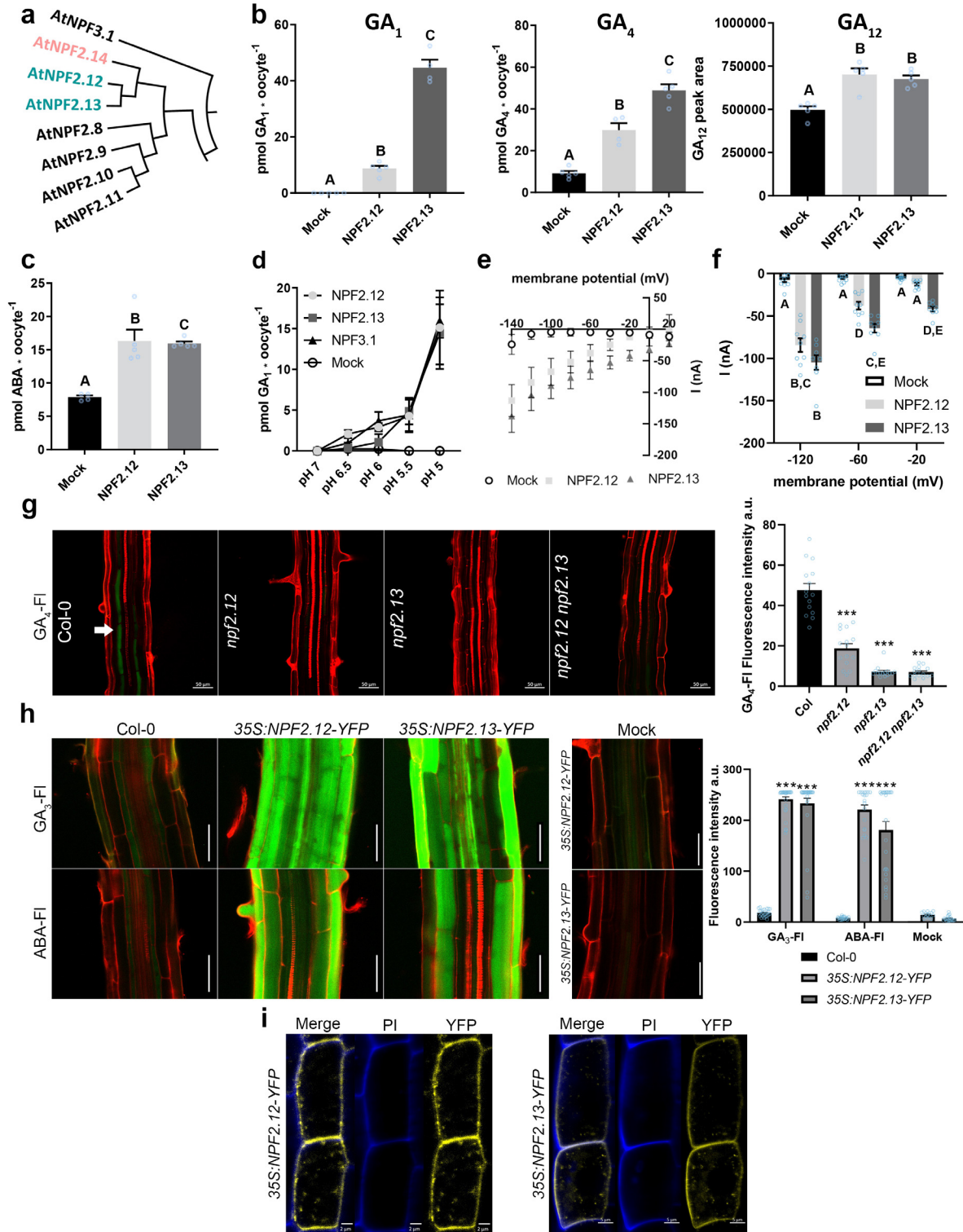


**Fig. 3. NPF2.12 and NPF2.13 are plasma membrane-localized GA and ABA importers that facilitate endodermal hormone accumulation.** (a) Phylogenetic clade of *NPF2.12*, *NPF2.13*, *NPF2.14*, and their close paralogs. (b and c) Hormone uptake in control and NPF2.12- and NPF2.13-expressing *Xenopus* oocytes. (b) Oocytes were exposed to 50  $\mu$ M  $GA_1$  at pH 5 (n = 5 single oocytes), 50  $\mu$ M  $GA_4$  at pH 5.5 (n

= 5), or 50  $\mu\text{M}$  GA<sub>12</sub> at pH 6 (n = 5). (c) Oocytes were exposed to 50  $\mu\text{M}$  ABA at pH 5 (n = 5). Hormone uptake was analyzed by LC-MS/MS. Statistical significance was assessed using Holm Sidak one-way ANOVA ( $p = 0.05$ ). (d) Oocytes were exposed to 50  $\mu\text{M}$  GA<sub>1</sub> at pH ranging from 5 to 7 (n = 5). (e and f) Control oocytes (n = 10), oocytes expressing NPF2.12 (n = 9), and oocytes expressing NPF2.13 (n = 8) were exposed to 500  $\mu\text{M}$  GA<sub>3</sub> at pH 5, and currents were measured using two-electrode voltage clamp electrophysiology over a range of membrane potentials from +20 to -140 mV. Statistical significance was assessed using Holm Sidak two-way ANOVA ( $p = 0.01$ ). (g) Left: Representative images of roots of 6-day-old Col-0 and single and double *npf2.12* and *npf2.13* knockout plants treated with 5  $\mu\text{M}$  GA<sub>4</sub>-Fl (green) overnight. Red indicates propidium iodide. The white arrow indicates GA<sub>4</sub>-Fl signal. Right: Quantification of GA<sub>4</sub>-Fl fluorescence intensity in the endodermis, mean  $\pm$  S.E. (5 endodermal cells were sampled from 3 biological repeats, n = 15). Significance was determined by Dunnett's multiple comparisons test (\*\*\*)  $p \leq 0.0001$ ). (h) Left: Representative images of roots of 6-day-old *35S:NPF2.12-YFP* and *35S:NPF2.13-YFP* plants treated with 5  $\mu\text{M}$  GA<sub>3</sub>-Fl and ABA-Fl for 2 hours. Red indicates propidium iodide, green indicates GA<sub>3</sub>-Fl or ABA-Fl. Right: GA<sub>3</sub>-Fl and ABA-Fl fluorescence intensity was quantified in the epidermal cells, mean  $\pm$  S.E. (5 epidermal cells sampled from at least 4 biological repeats, n > 20). *35S:NPF2.12-YFP* and *35S:NPF2.13-YFP* mock do not show fluorescence under these confocal gain settings. (i) Confocal imaging of 6-day old root meristem epidermis cells expressing *35S:NPF2.12-YFP* and *35S:NPF2.13-YFP*. Blue is PI, yellow is YFP.

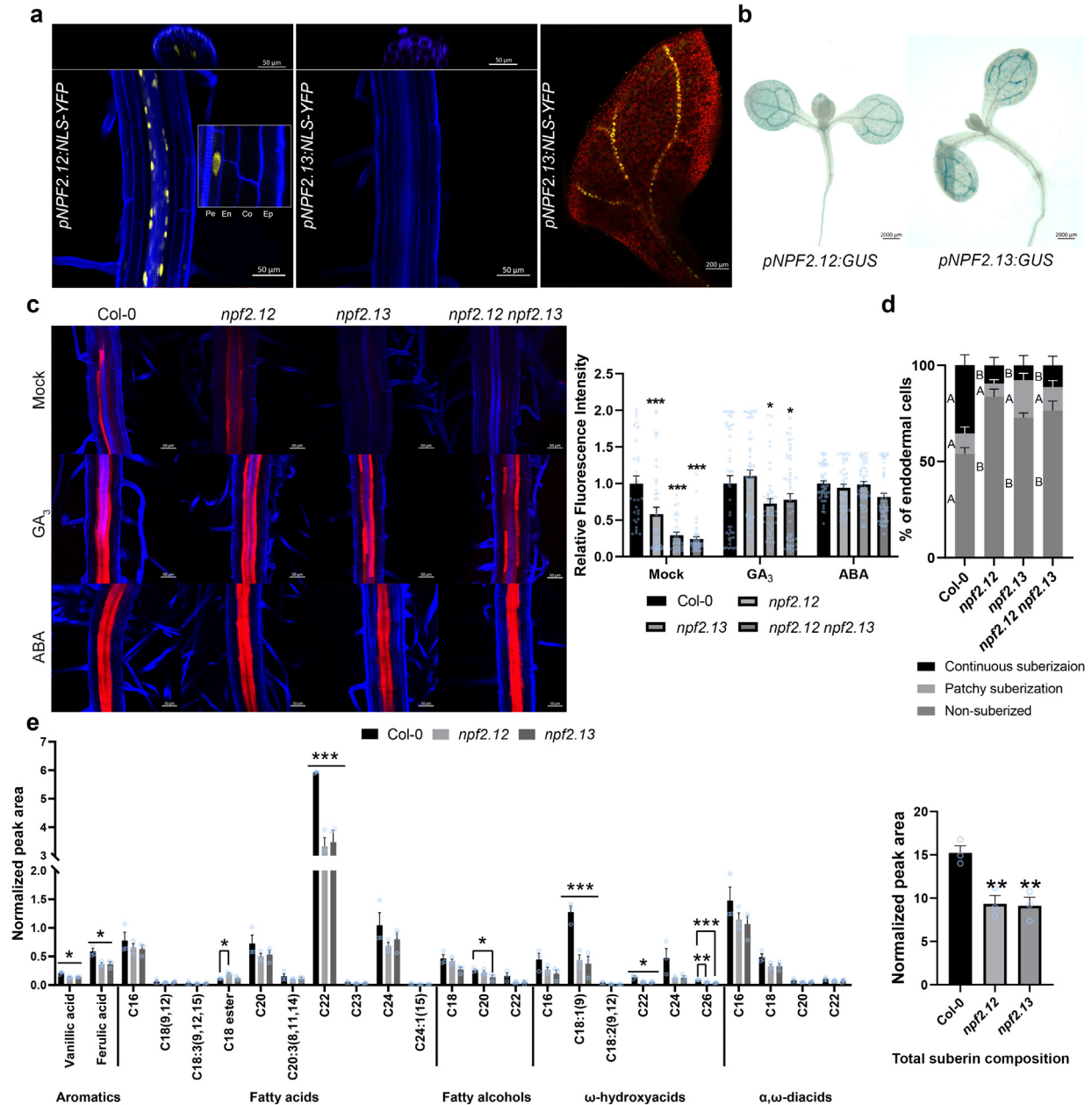


**Fig. 4. *NPF2.12* and *NPF2.13* regulate root endodermis suberization.** (a) Confocal imaging of 6-day-old *pNPF2.12:NLS-YFP* and *pNPF2.13:NLS-YFP* seedlings. Inset is magnification of cells with *pNPF2.12:NLS-YFP* signal. Pe – Pericycle, En - Endodermis, Co – Cortex, Ep – Epidermis. Blue indicates either calcofluor, yellow indicates YFP. Right image is *pNPF2.13:NLS-YFP* cotyledon (red indicates chlorophyll). (b) GUS staining of 7-day-old seedlings expressing *pNPF2.12:GUS* and *pNPF2.13:GUS*. (c) Left: Nile red-stained 5-day-old *npf* mutant roots mock treated or treated with 5  $\mu$ M GA<sub>3</sub> or 1  $\mu$ M ABA. Right: Fluorescent intensity relative to Col-0 quantified from a minimum of 8 roots per treatment, 5 endodermal cells per root,  $n > 40$ . Statistical significance was assessed using a Dunnett's test (\*  $p < 0.05$ , \*\*  $p < 0.01$ , \*\*\*  $p < 0.001$ ). (d) Quantifications of suberin pattern along the root using Nile red fluorescence intensity,  $n = 10$ . Different letters indicate significant differences between conditions ( $p < 0.05$ ). (e) Root suberin profile for 10-day-old plants, measured by gas chromatography-mass spectrometry. The y-axis represents relative peak areas following normalization to a C<sub>32</sub>-alkane internal standard. Right graph

indicates for total suberin composition. Data in bars represent the means  $\pm$  SE of three biological replicates. \* indicates statistically significant differences compared with Col-0 at  $p \leq 0.015$ , \*\*  $p \leq 0.01$  and \*\*\*  $p \leq 0.001$  by Student's t-test.

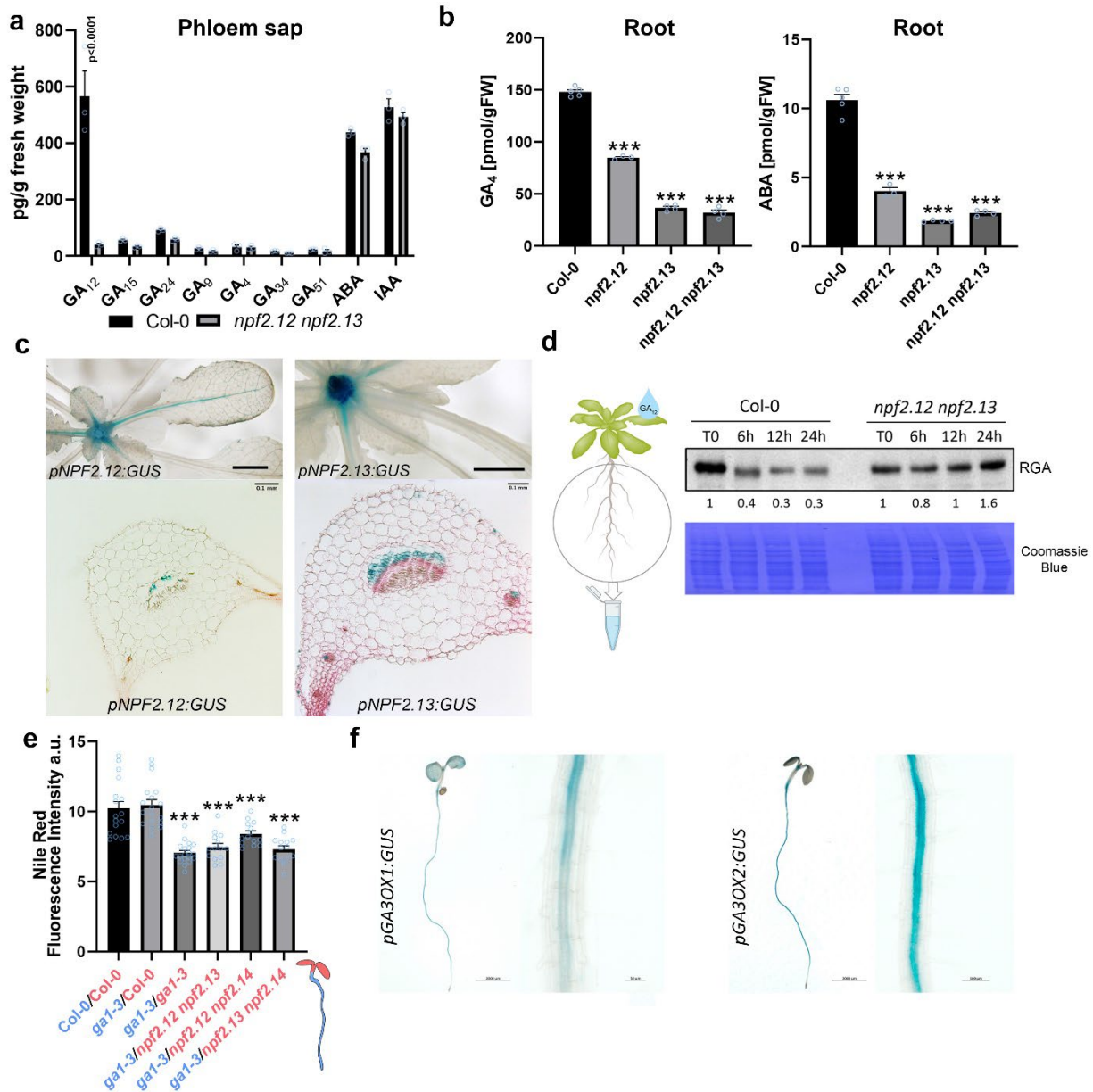


**Fig. 5. NPF2.12 and NPF2.13 facilitate long-distance shoot-to-root GA transport.** (a) Quantification of GA, ABA and IAA contents (in  $\text{pg}\cdot\text{g}^{-1}$  fresh weight) in phloem exudates collected from leaf petiole of 5-week-old Col-0 and *npf2.12 npf2.13* mutant plants. Exudate was collected from 75 leaves, pooled into 3 separate biological repetitions ( $n = 3$ ). Statistical significance evaluated by Dunnett's multiple comparisons test, comparing to Col as control. ( $p < 0.0001$ ) (b) GA<sub>4</sub> and ABA quantification (in  $\text{pmol}\cdot\text{g}^{-1}$  fresh weight) in 10-day-old roots of Col-0 and *npf2.12 npf2.13* double-mutant plants ( $n = 5$ ). Significance was assessed using Dunnett's multiple comparisons test (\*\*\*)  $p \leq 0.0001$ . (c) GUS staining patterns in rosette leaves of

4 week-old *pNFP2.12:GUS* and *pNPF2.13:GUS* plants. Top images are whole plants; scale bars represent 0.25 cm. Bottom images are cross-sections of GUS-stained leaf petioles; scale bars represent 0.1 mm. **(d)** Immunodetection of RGA protein accumulation in the root of 16-day-old Col-0 and *npp2.12 npp2.13* mutant plants. The plants were grown *in vitro* for 12 days and then moved to MS plates containing a low concentration of nitrogen (0.5 mM KNO<sub>3</sub>) and paclobutratol (PAC, 1 μM). 4 days after transfer, a drop of GA<sub>12</sub> (5 μl at 1 μM) was added to one of the first two leaves formed. Proteins were extracted from the root at 4-time points following GA<sub>12</sub> application. Similar results were obtained in two independent experiments. **(e)** Quantification of Nile red fluorescence intensity (mean ± s.d.; n ≥ 10) of various combinations of grafted seedlings. Blue font indicates for rootstock genotype, red indicates for grafted scion. Fluorescence intensity was quantified from a minimum of 10 roots per genotype/grafting, 5 endodermal cells per root, n > 50. Statistical significance was assessed using a Dunnett's test (\*\*\*) *p* < 0.001). **(f)** Images of 6-day-old plants that express GUS driven by the *GA3OX1-2* promoters.



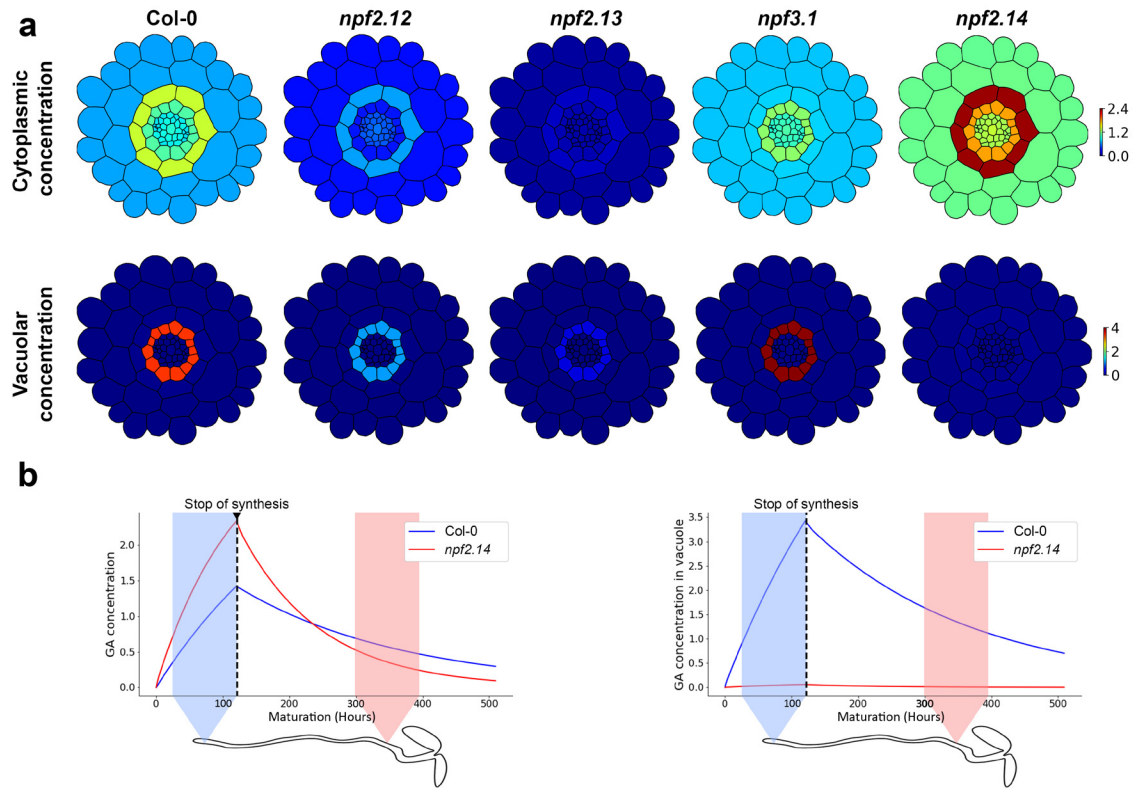


**Fig. 6. NPF transporters mediate pericycle-specific hormone uptake into the vacuoles at the phloem unloading zone to facilitate a hormone slow-release mechanism that allows suberization at the maturation zone.** (a) Spatial distributions of cytoplasmic and vacuolar GA concentration in the root cross-section, predicted by the multicellular mathematical model, for the wild type, and the *npf2.12*, *npf2.13*, *npf3.1*, and *npf2.14* mutants. The time of the simulations is 5 days (120 hours), corresponding to the age of the plants used in the experiments. (b) Predicted dynamics of the endodermal cytoplasmic and pericycle vacuolar GA concentration for the wild type and the *npf2.14* mutant. The model is initially simulated with a constant GA source in the stele (pale blue region), then synthesis is set to zero to simulate the GA redistribution after cells leave the phloem unloading zone. The model predicts that NPF2.14 leads to higher endodermal cytoplasmic concentrations where suberin forms (pale red region).

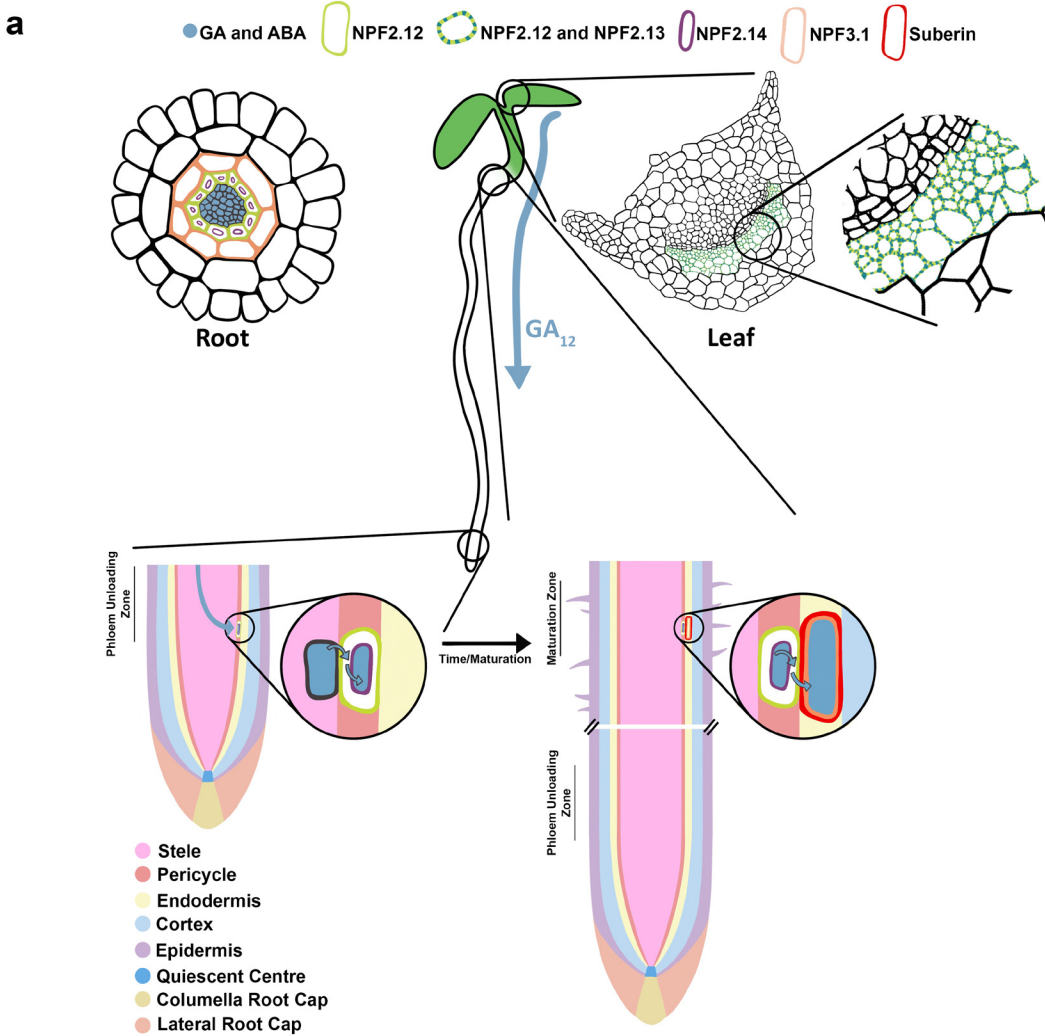


**Fig. 6. Proposed model illustrating NPF2.12, NPF2.13, NPF2.14 and NPF3.1 function in regulating endodermal suberin formation.** Proposed model incorporating experimentally observed distributions of root GA transporters, hormone accumulation, endodermal suberin formation and mathematical model predictions. NPF2.12 and NPF2.13, which are localized to the shoot phloem, are both required for  $GA_{12}$  long-distance shoot-to-root translocation. NPF2.12 is expressed in the root pericycle cell membranes and promotes the movement of ABA and GA from the vasculature to the pericycle. Once in the pericycle cytoplasm, NPF2.14 imports the hormones into the vacuole to form a reservoir which will be available in later stages. When the root elongates over time and the cells that accumulated high levels of GA and ABA in the vacuoles mature, the hormones are exported out of the pericycle vacuole and imported into the endodermis by NPF3.1 to induce suberization.